



OPEN ACCESS

EDITED BY

Qiuming Pei,
Southwest Jiaotong University, China

REVIEWED BY

Xinkai Hu,
Second Institute of Oceanography, Ministry of
Natural Resources, China
Xiaochao Shu,
China University of Mining and Technology,
China

*CORRESPONDENCE

Pan Tang,
✉ tangpan168@163.com
Haifeng Li,
✉ mcchaifengli@163.com

RECEIVED 30 January 2024

ACCEPTED 04 April 2024

PUBLISHED 19 April 2024

CITATION

Li F, Tang J, Song Y, Li S, Tang P, Li H, Yang H, Wang Q, Wang Y, Danzeng Z, Li Y, Li J, Li H and Dong Y (2024), Major elements geochemistry of chlorite in different ore deposits and its genesis and exploration significance: a case study from Naruo porphyry Cu deposit in Duolong ore district, Tibet.

Front. Earth Sci. 12:1378820.
doi: 10.3389/feart.2024.1378820

COPYRIGHT

© 2024 Li, Tang, Song, Li, Tang, Li, Yang, Wang, Wang, Danzeng, Li, Li, Li and Dong. This is an open-access article distributed under the terms of the [Creative Commons Attribution License \(CC BY\)](#). The use, distribution or reproduction in other forums is permitted, provided the original author(s) and the copyright owner(s) are credited and that the original publication in this journal is cited, in accordance with accepted academic practice. No use, distribution or reproduction is permitted which does not comply with these terms.

Major elements geochemistry of chlorite in different ore deposits and its genesis and exploration significance: a case study from Naruo porphyry Cu deposit in Duolong ore district, Tibet

Faqiao Li¹, Juxing Tang², Yang Song¹, She Li³, Pan Tang^{4*}, Haifeng Li^{5*}, Huanhuan Yang¹, Qin Wang⁶, Yongqiang Wang⁷, Zongzhui Danzeng⁷, Yanbo Li⁸, Jianli Li⁸, Hongwei Li⁸ and Yujie Dong⁸

¹Ministry of Natural Resources Key Laboratory of Metallogeny and Mineral Assessment, SinoProbe Laboratory, Institute of Mineral Resources, Chinese Academy of Geological Sciences, Beijing, China, ²SinoProbe Laboratory, Chinese Academy of Geological Sciences, Beijing, China, ³Golden Dragon Mining Co., Ltd., Lhasa, Tibet, China, ⁴SinoProbe Laboratory, Southwest University of Science and Technology, Mianyang, Sichuan, China, ⁵China 19th Metallurgical Corporation, Chengdu, Sichuan, China, ⁶College of Earth Sciences, Chengdu University of Technology, Chengdu, Sichuan, China, ⁷Tibet University, Lhasa, Tibet, China, ⁸No. 5 Geological Party, Tibet Bureau of Geology and Mineral Exploration and Development, Golmud, Qinghai, China

Chlorite is present extensively in many types of deposits. The mechanism underlying the chemical variations in chlorite remains unclear. The Naruo porphyry deposit is a giant copper porphyry deposit in the Duolong ore district of Tibet. Chlorite, which is abundant in this deposit, has yet to be studied systematically; hence, we used principal component analysis (PCA) to assess the correlation between chlorite elements and various types of mineral deposits. We then conducted a preliminary investigation into its mineralogy and geochemistry to better understand its formation process and identify potential prospecting indicators. The PCA method proved effective in discerning two distinctive element signatures within the chlorite and categorising them into four deposit types: orogenic Au deposits, granite-type U deposits, and skarn-type Sn deposits that exhibit high FeO and low MgO distinguishing them from porphyry copper deposits. The chlorite in the Naruo deposit is classified as either early metasomatic (M-type), consisting mainly of clinochlore, or late hydrothermal (H-type), primarily consisting of clinochlore and chamosite. This classification suggests that H-type chlorite formed in a reductive environment conducive to Cu precipitation at medium temperatures (255°C–342°C). Al-Si and Fe-Mg substitutions were found to be the primary processes involved in its generation. Additionally, from the mineralisation centre outwards, there was an observed decrease in Si content as well as the Fe/(Fe+Mg) ratio in H-type chlorite, along with decreases in temperature, sulphur, and oxygen fugacity of all chlorites; conversely,

increases were observed for Al content along with Mg and Mn elements in H-type chlorite. Chlorite is useful for exploring porphyry copper systems as an indicator mineral.

KEYWORDS

chlorite, mineralogy, metallogeny, principal component analysis, prospecting, porphyry copper deposit, Tibet

1 Introduction

Chlorite is a common alteration mineral that can be found in sedimentary, low-grade metamorphic, and hydrothermally altered rocks, among multiple types of rocks and geological settings (De Caritat et al., 1993; Vidal et al., 2001; Yavuz et al., 2015), especially some Cu, Au, and U deposits (Sillitoe et al., 2010; Zhong et al., 2011; Wilkinson et al., 2015). Chlorite's typical crystallochemical formula is represented by $(R_x^{2+}R_y^{3+}F2A5_{6-x-y})_6^{VI}(Si_{4-z}R_z^{3+})_4^{IV}O_{10}(OH)_8$, where R_x^{2+} = Fe²⁺, Mg²⁺, Mn²⁺, Co²⁺, Ni²⁺, Zn²⁺ and Cu²⁺; R_y^{3+} = Al³⁺, Fe³⁺, ±Cr³⁺, ±V³⁺; F2A5= octahedral vacancy; R_z^{3+} = Al³⁺, ±B³⁺, ±Fe³⁺ (Yavuz et al., 2015; Zane et al., 1998). The chemical formula demonstrates that chlorite mineral has a wide range of stoichiometric compositions, and its chemical composition changes are influenced by the temperature, pressure, and physicochemical conditions of the whole-rock compositions during chlorite formation (Bourdelle et al., 2013; Inoue et al., 2009; Vidal et al., 2000). Hence, the chemical elements of chlorite can be used to calculate the temperature, oxygen fugacity, sulphur fugacity, and other environmental conditions during its formation (Cathelineau et al., 1985; Walshe et al., 1986; Kranidiotis et al., 1987; Xie et al., 1997; Battaglia, 1999; Inoue et al., 2009; Chang et al., 2011; Bourdelle et al., 2013; Bourdelle, 2021). The geochemical elements and isotopes of altered minerals (such as chlorite and epidote) can now be widely used in the study of the genesis, prospecting, and exploration of various types of deposits, owing to the development of *in situ* testing and analysis technologies, such as EPMA and LA-ICP-MS, as well as improvements in testing accuracy (Chang et al., 2011; Wilkinson et al., 2015; Cooke et al., 2020; Pacey et al., 2020; Fan et al., 2021). However, distinct differences in chlorite elements between various metal deposits are yet to be determined.

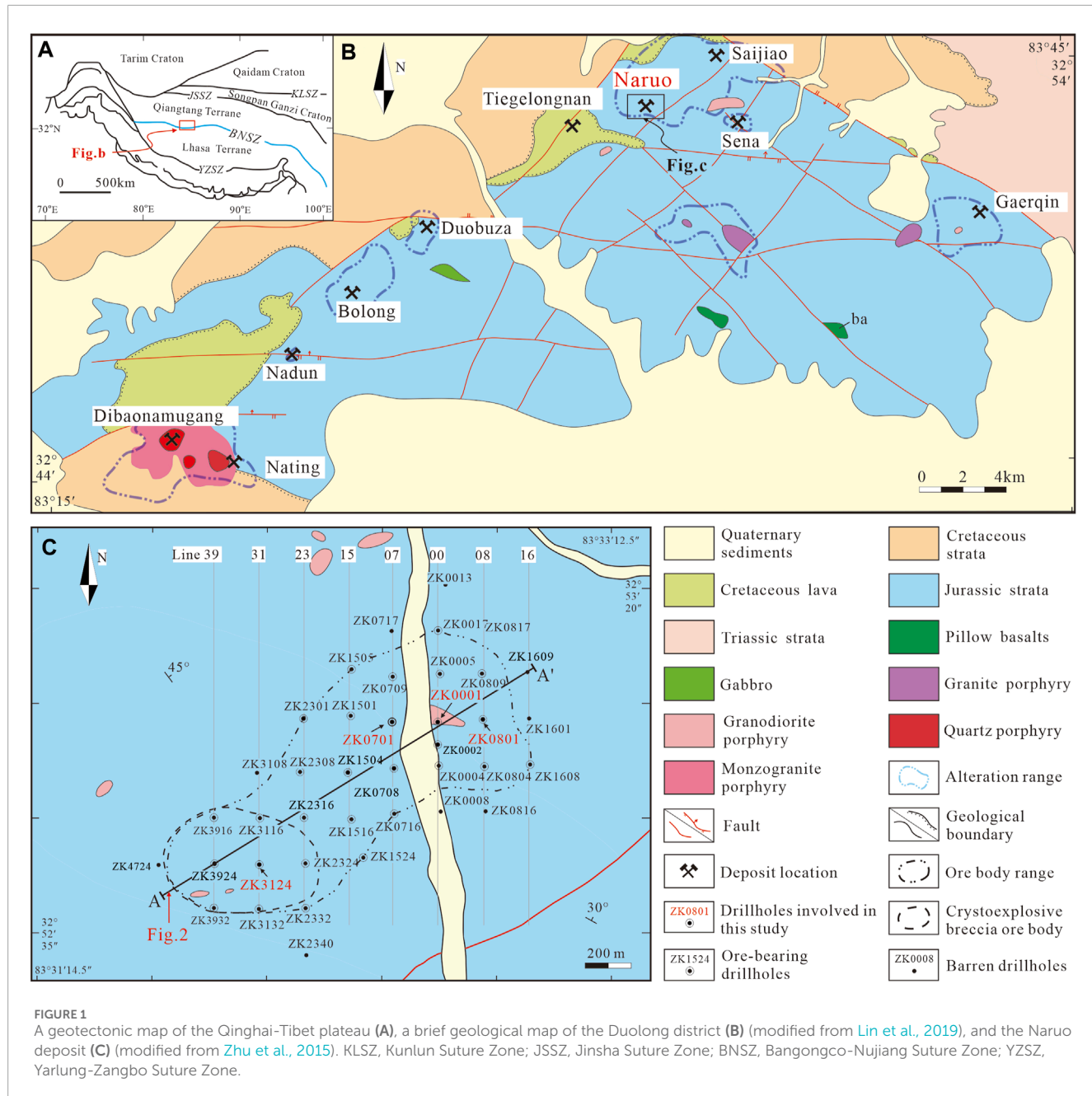
The Bangonghu-Nujiang metallogenic belt, alongside the Gangdise belt (Sun et al., 2023; Lin et al., 2024), is one of the pivotal metallogenic belts in Xizang and has recently been marked by significant advancements in ore prospecting. Among these, the Duolong Ore District emerged as the primary contributor. Notably, the Naruo deposit represents a substantial large-scale porphyry Cu deposit within this region (Figures 1A,B), with Cu resources exceeding 2.5 million tons and associated Au resources exceeding 80 tons (Tang et al., 2017; Lin et al., 2019). Several studies on the geochronology of diagenesis and metallogenesis, magmatic petrogenesis, and metallogenic dynamic settings have been the primary subjects of earlier studies that have achieved significant progress (Ding et al., 2014; Sun et al., 2015; Zhu et al., 2015; Bai et al., 2016; Ding et al., 2017; Lin et al., 2019; Zhu et al., 2019; Gao et al., 2021). However, little research has been conducted on the mineralogy of chlorite, which is one of the most widely distributed minerals in the Naruo deposit and is closely related

to mineralisation (Lin et al., 2019; Li, 2022). Yang et al. (2015) studied the chlorite in the Naruo deposit, including its mineralogy and geochemistry, and discussed the relationship between some chlorite elements and mineralisation to guide prospecting and exploration. Nevertheless, the study of the classification and elemental geochemistry of chlorite is relatively preliminary and fails to give full play to the maximum utilisation of chlorite minerals in the genesis of the deposit and the prospecting and exploration of indicators.

In this study, we collected chlorite data from prior studies on Cu, Au, U, and Sn deposits to evaluate their compositions and determine the compositional differences using PCA. Mineralogy and elemental geochemistry were used to produce a more precise mineralogical and geochemical classification of the chlorite in the Naruo deposit. This helps to clarify the origin of the deposit and provides significant insights for future prospecting and exploration efforts.

2 Regional geological background

The Bangongco-Nujiang suture zone (BNSZ) stretches through the middle of the Qinghai Tibet Plateau, representing the remnants of the Bangongco-Nujiang Tethys Ocean after its closure (Yin et al., 2000), and is also the boundary between the Qiangtang and Lhasa terranes (Figure 1A) (Li, 1987; Li et al., 2008; Pan et al., 2011). It has recently developed into one of Tibet's three main metallogenic belts, the Bangongco-Nujiang metallogenic belt, due to multiple mineral exploration breakthroughs in the region (Tang et al., 2014; Tang et al., 2014; Tang et al., 2016; Lin et al., 2017; Tang et al., 2017). Duolong, the most representative porphyry-epithermal copper polymetallic ore district, is located in the western section of the BNSZ (Figure 1A). The Duolong district comprises four large-to-giant-sized deposits, two medium-sized deposits, and several mineralisation spots (Figure 1B). Cumulative identified and potential Cu resources exceed 25 million tons. The associated Au and Ag resources are more than 400 tons and 3,500 tons, respectively, making the Duolong district a world-class copper polymetallic ore district (Tang et al., 2017). The stratigraphic units in the Duolong district mainly include the limestone within the Upper Triassic Riganpeicuo Formation (T_3r), covered by the sandstone, siltstone of the Lower Jurassic Quse Formation (J_1q), and the lithic quartz sandstone of the Middle Jurassic Sewa Formation (J_2s), overlain by andesite and dacite of the Lower Cretaceous Meiriqiecuo Formation (K_1m), and the sandstone, conglomerate of the Upper Cretaceous Abushan Formation (K_2a) through fault (Figure 1B). The mineralisation-related strata are mainly sandstone and siltstone of the Quse and Sewa Formations and andesite from the Meiriqiecuo Formation.

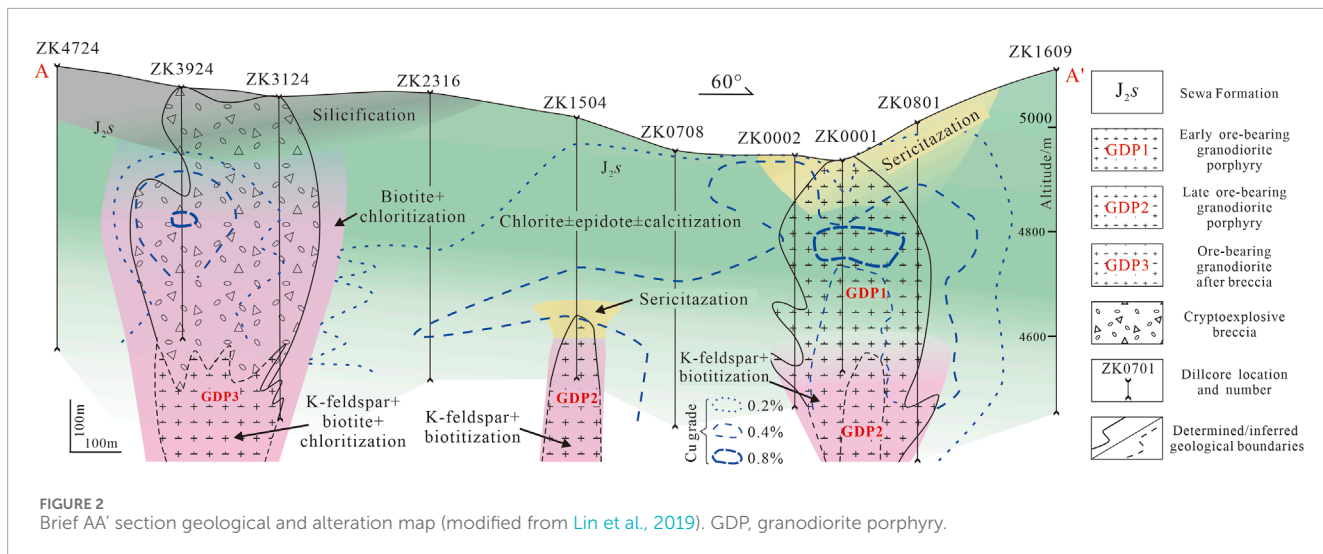


The fault structures in the district are divided into three groups, namely, the E-W fault before mineralisation, the NW ore-controlling fault, and the NE fault structure after mineralisation, forming the ‘diamond’ structure framework jointly (Figure 1B) (Lin et al., 2019; Wang et al., 2019). This type of structural framework provides a favourable environment for magma emplacement. Consequently, there was more magmatic activity during the Yanshan period, which was characterised by intermediate to acidic magmatic rocks. Basic, intermediate-felsic, and felsic magmatic activities also occurred. Basic volcanic rocks are covered by fissure- and overflow-type eruptions, and intermediate-felsic magmatic rocks primarily intrude into the Jurassic strata in the form of rock branches and dikes (Figure 1B); these magmatic rocks formed in an arc environment caused by the northward subduction of the Bangongnu-Nujiang

Tethys Ocean (Li et al., 2016; Tang et al., 2016; Lin et al., 2017; 2019; Li et al., 2022).

3 Geology of the Naruo deposit

The Naruo deposit is the third-largest porphyry Cu (Au) deposit in the Duolong ore district. The second member of the Middle Jurassic Sewa Formation ($J_2 s_2$) feldspathic quartz sandstone, which is a flysch-like-to-flysch formation in a passive continental margin setting, comprises most of the developed strata in Naruo and is an ore-bearing strata (Figure 1C). No obvious ore-controlling fault was identified on the surface; however, the possibility of deep existence cannot be ruled out. Although less visible on the surface (Figure 1C), the magmatic



activity of the Naruo deposit was developed and revealed through drilling engineering. The magmatic rocks related to mineralisation are mainly granodiorite porphyry in the form of columnar stock-like bodies and have been dated to ca. 122–116 Ma (Sun et al., 2015; Zhu et al., 2015; Ding et al., 2014; Bai et al., 2016; Gao et al., 2017; Lin et al., 2019; Zhu et al., 2019). The barren intrusions are mainly composed of granodiorite porphyry (~116 Ma) to the north and diorite (~121 Ma) to the east of the deposit (Zhu et al., 2015). The geochemistry and isotopic characteristics of the entire rock revealed that Naruo ore-bearing magma was formed under the background of the northward subduction of the Bangongcu-Nujiang Tethys Ocean (Ding et al., 2014; Zhu et al., 2015; Li et al., 2016; Gao et al., 2017; Lin et al., 2019; Zhu et al., 2019). The orebody of the Naruo deposit is separated into porphyry and crypto-explosive breccia metallogenetic systems and is dispersed in a NE-SW direction (Figure 1C). Currently, there are more than 2.5 million tons of identified and potential copper metal resources, more than 80 tons of gold, and approximately 900 tons of silver.

From the centre to the periphery, the alteration zoning of the Naruo deposit can be roughly divided into potassium feldspar alteration, sericitization, propylitization, high-grade argillization, and silicification (Figure 2A). However, many controversies exist regarding the classification of alteration types, the location of alteration zoning, and the sequence of alteration development (Ding et al., 2014; Sun et al., 2015; Sun et al., 2015; Yang et al., 2015; Zhu et al., 2015; Gao et al., 2016; Lin et al., 2019; Zhu et al., 2019). One view suggests that mineralisation develops in the potassium alteration zone (Sun et al., 2015), whereas the opposite view holds that mineralisation develops in the propylitic alteration zone (Yang et al., 2015; Lin et al., 2019). In this study, large-scale chloritization developed in the porphyry and crypto-explosive breccia systems of the Naruo deposit (Figure 2), and chalcopyrite mineralisation was mostly associated with chlorite (Figures 3A–D). The chloritization alteration developed near the mineralisation centre of the porphyry system (Figures 3A,B). Similarly, the crypto-explosive breccia system also developed a strong chloritization alteration, mainly in the breccia interstitial matrix and breccia (Figures 3C,D). These conclusions coincide with those of previous

studies showing that Cu mineralisation is mostly related to chlorite alteration (Yang et al., 2015; Lin et al., 2019).

4 Mineralogical classification of chlorite

Different methods are used for the mineralogical classification of chlorite minerals in different deposits. Yang et al. (Yang et al., 2015) classified the chlorite in the Naruo deposit into four categories based on its appearance: type I is chlorite in the crypto-explosive breccia system, type II is chlorite in the porphyry system, type III is chlorite in feldspar quartz sandstone, and type IV is chlorite in the form of vein. Several metallogenetic systems of the Naruo deposit have been studied in detail using this categorisation technique, which has several advantages. According to the order of alteration of the porphyry Cu deposits, Xiao et al., 2018, 2017) separates the chlorite in the Yandong and Tuwu porphyry Cu deposits in Xinjiang into two phases, namely, the propylitization and the supergene stage. The geochemical properties of chlorite can now more accurately represent the mineralisation process owing to this categorisation approach. Other researchers have classified chlorite according to its degree of alteration, which may clearly illustrate the coupling relationship between the degree of alteration (mineralisation) and some indicative geochemical components of chlorite (Zhang et al., 2014; Wang et al., 2018).

In this study, the chlorite in the Naruo deposit was separated into the primary early metasomatic type (M-type) and the late hydrothermal precipitation type (H-type) by combining extensive core geological logging and polished thin section observations. The M-type is mainly schistose chlorite formed by early metasomatic mafic minerals such as amphibole and biotite (Figures 3F–H), which are widely developed in ore-bearing intrusions throughout the deposit. This type of chlorite mainly presents a metasomatic residual or pseudotexture (Figure 3H), and the associated minerals include quartz, magnetite, pyrite, and chalcopyrite (Figures 3F–H). The H-type is mainly scaly and vermicular chlorite formed by dissolution and precipitation, which are interspersed in early minerals in veined form or developed in the mineral gap of the

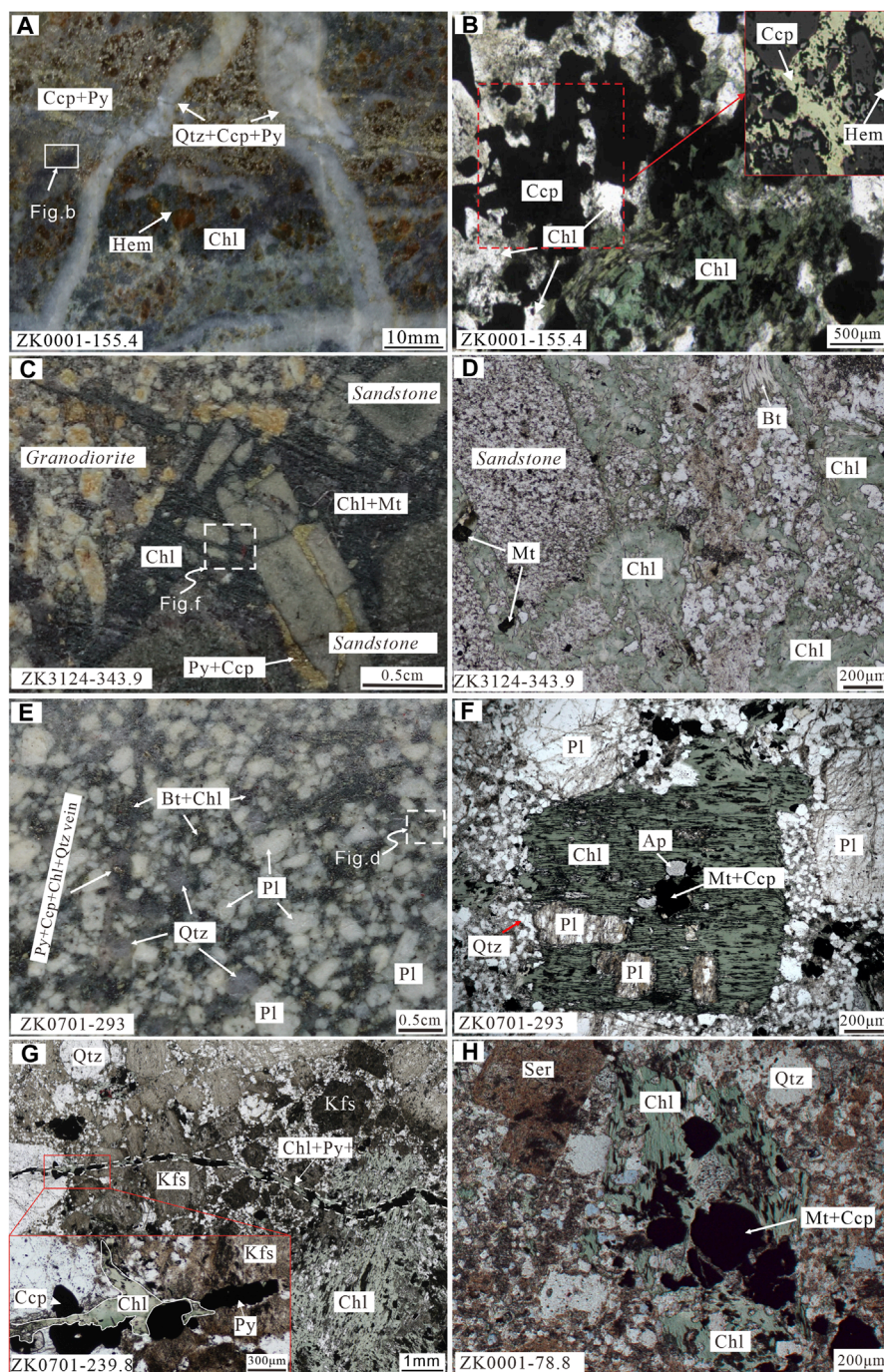


FIGURE 3

Drill core specimen photographs and microscopic photographs of typical samples in the Naruo deposit. **(A)** ZK0001-155.4, earlier chalcopyrite+pyrite coarse veins, later quartz+chalcopyrite+pyrite veins and chlorite developed at the centre of the porphyry metallogenetic system; **(B)** The microscopic photo corresponding to Figure **(A)** show the development of chalcopyrite mineralization and chloritization alteration; **(C)** ZK3124-343.9m, the breccia in crypto-explosive breccia system is mainly composed of granodiorite porphyry and sandstone; Strong hydrothermal type of chlorite can be seen in matrix and breccia of sandstone and granodiorite; Mineralization is characterized by the development of a large amount of magnetite and a small amount of brass and pyrite; **(D)** Strong chlorite alteration is developed. Hydrothermal type of chlorite is filled in the matrix and coexists with magnetite; **(E)** ZK0701-293m, granodiorite porphyry in the porphyry Cu system developed an obvious metasomatic type of chlorite alteration and disseminated, vein pyrite and chalcopyrite; **(F)** The metasomatic type of chlorite; it shows the metasomatic pseudomorphous structure, with biotite framework still visible, and chlorite coexists with magnetite, plagioclase, and apatite; **(G)** Metamorphic chlorite is cut through by hydrothermal vein chlorite, indicating that the latter was formed earlier than the former; **(H)** The metasomatic type of chlorite, which was formed from metasomatizing hornblende, showing the metasomatic pseudo structure and coexisting with magnetite and chalcopyrite. Qtz, quartz; Pl, plagioclase; Bt, biotite; Ap, apatite; Chl, chlorite; Py, pyrite; Ccp, Chalcopyrite; Mt, magnetite; Hem, hematite.

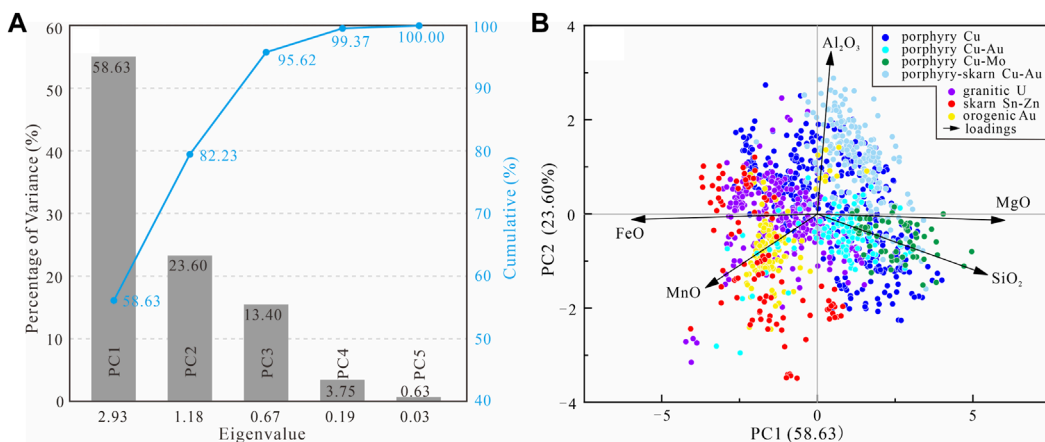


FIGURE 4

Compositional eigenvalues and cumulative proportion (A), and score and loading plots (B) of the chlorites with different origins. Black vector lines represent the PC loadings for the elements. Data on porphyry Cu deposit was from Xiao et al. (2017), Sun et al. (2015), Wang et al. (2014); porphyry Cu-Au deposit was from Yang et al. (2015), Zhang et al. (2020) and this study; porphyry Cu-Mo deposit was from Feng et al. (2022), Tang (2022); porphyry Cu-Mo-Au deposit was from Li (2021); granitic U was from Wu et al. (2018), Qin et al. (2018), Zhang et al. (2018), Wang et al. (2018), Xu et al. (2017), Zhang et al. (2007); skarn-type Sn was from Liu et al. (2022), Liao et al. (2010); orogenic Au was from Zhou et al. (2018), Zheng et al. (1997), Xiao et al. (1993).

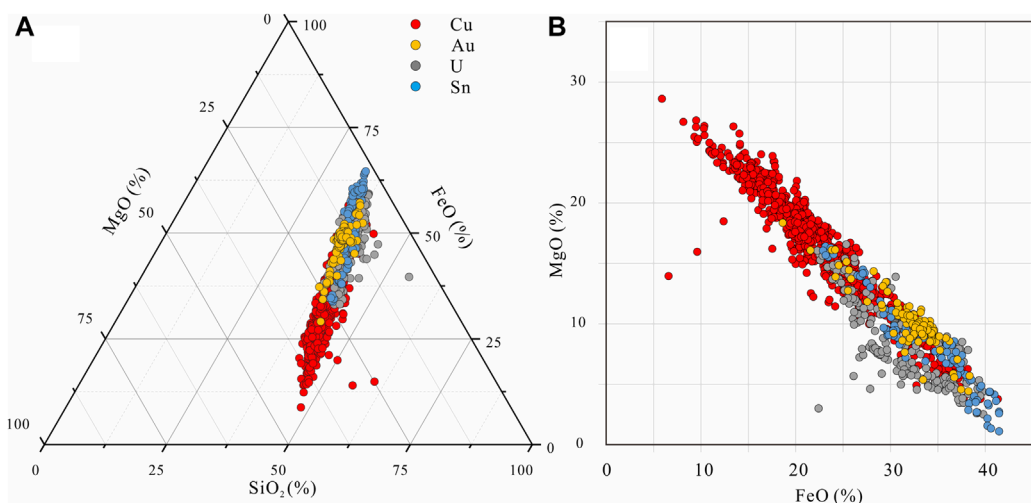


FIGURE 5

Ternary diagram (A) of SiO₂-FeO-MgO and binary diagram of FeO-MgO (B) in chlorite from different hydrothermal metal deposits.

wall rock in a disseminated form, coexisting with quartz, pyrite, and chalcopyrite (Figures 3A–D,G). This type of chlorite is mainly developed in porphyry copper ore systems and crypto-explosive breccia mineralisation centres.

system (the marked red drill holes in Figure 1) based on thorough cataloging. Following detailed microscopic mineral identification, *in situ* EPMA major elements testing of chlorite was then performed.

The test was performed on thin slices at the Electron Probe Laboratory of the Institute of Mineral Resources, Chinese Academy of Geological Sciences. The model of the experimental instrument was JXA-8230, and the specific experimental conditions were, an acceleration voltage of 15 kV, current of 20 nA, and beam spot diameter of 5 μm. During the test and analysis, the Si, Na, and Al contents were tested with a jadeite standard sample, and the contents of Mg, K, Ca, Fe, Ti, Mn, Cr, and P elements were tested with forsterite, potassium feldspar, wollastonite, haematite, rutile, manganese oxide, chromium oxide, and apatite standard samples.

5 Methods and results

5.1 Methods

This study primarily collected samples from ZK0001, ZK0701, and ZK0801 in the porphyry metallogenetic system of the Naro deposit and ZK3124 in the cryptoexplosive breccia metallogenetic

The test points avoided fractures and other mineral inclusions in the chlorite minerals.

Principal Component Analysis (PCA) is a widely used statistical technique that transforms high-dimensional data into a new coordinate system by capturing the maximum variance in the first few principal components. This method was employed to simplify complex datasets and reveal the underlying patterns in the data (Jolliffe et al., 2002; Hu et al., 2022). PCA simplifies the data by replacing the original variables with a reduced set, preserving the maximum information through correlation, and explaining significant relationships in the first two principal components. This study compiled 1,208 primary elemental data points of chlorite in publicly disclosed porphyry-type Cu-polymetallic deposits in China (a reference to raw data can be found in the note of Figure 5), using the major elemental content of the chlorite formed in the sedimentary rocks as the reference value. Before conducting the PCA, values below the detection limit or equal to zero were excluded. And the dataset used in this study met the criterion of w ($\text{Na}_2\text{O} + \text{K}_2\text{O} + \text{CaO}$) < 1 wt% (>90% of the data were limited to <0.5 wt%) to exclude contamination by other minerals (Li et al., 2022). Because Na_2O , K_2O , and CaO mainly originate from other minerals intermixed in chlorite, F and Cl are volatile components, and EPMA cannot directly determine Fe_2O_3 , this study chose higher-content elements, namely, SiO_2 , Al_2O_3 , FeO , MnO , and MgO , as the subjects for the principal component analysis to minimise errors.

5.2 Results

5.2.1 Principal component analysis

The results of PCA are shown in Figure 4A. The cumulative variance contribution rate of the first two principal components (PC1: 58.63, PC2: 23.60) accounted for 82.23%, indicating that the distinguishing characteristics of the chlorite from the various deposits were prominently separated on the PC2 vs PC1 planes (Figure 4B). FeO , SiO_2 , and MgO contributed the most to PC1, whereas Al_2O_3 , MnO , and SiO_2 were the main contributors to PC2 (Figure 4B). Clearly, chlorite within the ore deposits of various metal types manifested distinct elemental attributes (Figure 4B). The porphyry Cu-polymetallic deposit strongly correlated with Al_2O_3 , MgO , and SiO_2 , concentrated mainly in the first, second, and fourth quadrants (blue, cyan, green, and light blue dots in Figure 4B). SiO_2 was the primary factor associated with U deposits distributed throughout the second, third, and fourth quadrants (purple dots in Figure 4B). FeO and MnO are key elements linked to the Sn-polymetallic deposits and are primarily found in the second and third quadrants (red dots in Figure 4B). The distribution of porphyry Cu-Au deposits overlaps that of orogenic Au deposits (cyan and yellow dots in Figure 4B).

5.2.2 Major elements

Because of the complex structure of chlorite and other associated minerals and inclusions in the mineral, it was necessary to eliminate the influence of contamination effects on the obtained EPMA data. Contaminated chlorites often exhibit high values of $(\text{CaO} + \text{Na}_2\text{O} + \text{K}_2\text{O}) > 0.5$ wt% (Foster, 1962; Inoue et al., 2010); therefore, it is necessary to exclude the data on this feature before discussion. After excluding unqualified data, the contents of the major elements in the 129 chlorite minerals are listed in

Table 1. The main oxide contents are as follows: M-type chlorite contains $\text{SiO}_2 = 26.79\text{--}31.00$ wt%, $\text{Al}_2\text{O}_3 = 17.70\text{--}21.98$ wt%, $\text{MgO} = 14.22\text{--}20.83$ wt%, $\text{Fe}_2\text{O}_3 = 0.29\text{--}3.48$ wt%, $\text{FeO} = 14.24\text{--}24.09$ wt%, $\text{MnO} = 0.27\text{--}2.13$ wt%; Comparatively, H-type chlorite has lower $\text{SiO}_2 = 24.93\text{--}30.13$ wt%, higher $\text{Al}_2\text{O}_3 = 17.66\text{--}21.43$ wt%, lower $\text{MgO} = 7.96\text{--}19.17$ wt%, same $\text{Fe}_2\text{O}_3 = 0.53\text{--}3.70$ wt%, higher $\text{FeO} = 17.15\text{--}30.35$ wt%, $\text{MnO} = 0.37\text{--}2.19$ wt%. Both M- and H-type chlorites have low CaO , Na_2O , K_2O , and Cr_2O_3 contents. The atomic number of each element was calculated using WinCcac based on 14 oxygen atoms (Yavuz et al., 2015). The atomic numbers of each element are listed in Table 2.

Data were calculated using WinCcac software based on 14 oxygen atoms (Yavuz et al., 2015), and the calculation formulas of oxygen fugacity and sulphur fugacity were calculated using the six-component solid solution model formula proposed by Walshe (1986) (for detailed calculation steps, please refer to Zhang et al., 2014); the calculation formula of chlorite thermometer (t) proposed by Kranidiotis and Maclean (1987) was used for the calculation of oxygen and sulphur fugacity.

6 Discussion

6.1 Major elemental characteristics of chlorite in different types of metal deposits

The diverse chemical composition of chlorite is a valuable indicator of the physicochemical conditions during its formation. Consequently, they play a crucial role in characterising the hydrothermal alteration process and estimating the temperature of ore formation (Yavuz et al., 2015; Cathelineau, 1988), particularly for Cu, Au, and U deposits (Sillitoe et al., 2010; Zhong et al., 2012; Wilkinson et al., 2015; Deer et al., 1963). Therefore, we propose that elemental profiling of chlorite is a pivotal methodology for classifying diverse categories of hydrothermal metal deposits.

The score plots (Figure 4B) illustrate the varying degrees of clustering among the four deposit types in close proximity to the origin. Differentiation among the four metal deposit types was primarily observed along the principal component 1 (PC1) direction. The loading diagram (Figure 4B) indicates that FeO and MgO exhibited the smallest and most extended angles in the PC1 direction, highlighting their substantial role in classifying the four types of metal deposits, followed by SiO_2 and MnO . We systematically identified the key elemental factors pivotal for categorising the four distinct types of metal deposits and subsequently created comprehensive plots (Figure 5) to visualise their significance. Our findings highlight the substantial influence of SiO_2 , FeO , and MgO in the chlorite on classifying these diverse metal deposits. In the ternary diagram (Figure 5A), SiO_2 exhibits a linear trend, whereas the spatial positions of MgO and FeO vary among the four types of deposits. The chlorite range in Cu deposits exhibits significant breadth, whereas Au, U, and Sn deposits are primarily concentrated in regions characterised by elevated FeO and diminished MgO . Furthermore, their respective ranges overlapped. A more in-depth analysis of the binary diagram (Figure 5B) reveals that within copper deposits, the distribution of FeO in chlorite is predominantly concentrated within the range of 5%–40%, whereas

TABLE 1 Major elements of chlorite in the Naruo deposit.

Sample ID.	Type	Distance (m)	Major elements (%)										
			SiO ₂	Al ₂ O ₃	MgO	Fe ₂ O ₃	FeO	MnO	TiO ₂	CaO	Na ₂ O	K ₂ O	Cr ₂ O ₃
841.8-3	M	706	28.80	18.97	15.32	2.16	20.80	2.03	0.04	0.06	0.01	0.04	0.10
841.8-4	M	706	28.70	19.04	15.70	1.94	20.30	1.96	0.06	0.09	0.04	0.01	0.59
841.8-7	M	706	28.23	18.96	16.38	1.07	21.78	2.09	0.10	0.05	—	—	0.09
841.8-8	M	706	28.28	20.22	17.93	1.50	19.70	0.52	0.03	—	0.03	0.02	0.02
841.8-9	M	706	28.23	20.00	17.29	1.41	20.88	0.56	0.07	—	—	—	0.08
841.8-1	M	706	27.89	20.24	17.07	1.11	21.56	0.53	0.04	0.02	0.02	0.01	0.02
841.8-11	M	706	28.06	20.31	17.77	1.42	19.92	0.58	0.07	—	0.01	0.02	0.02
841.8-13	M	706	27.93	19.88	17.12	1.08	21.59	0.57	0.03	0.03	—	0.02	0.06
841.8-14	M	706	28.50	19.83	17.84	1.50	20.09	0.53	0.03	0.01	0.02	0.01	0.05
841.8-15	M	706	28.69	20.34	17.37	1.93	19.42	0.50	0.03	0.01	—	0.02	0.01
169.4-3	M	197	28.80	18.46	16.42	1.46	22.64	0.77	0.02	0.02	—	—	0.04
169.4-4	M	197	29.39	18.63	17.17	1.80	20.62	0.74	0.10	0.01	0.01	0.02	—
169.4-5	M	197	28.58	19.42	16.88	1.83	20.46	0.71	—	0.07	0.03	0.01	0.13
669.5-1	M	543	30.60	17.70	17.77	2.35	19.19	0.36	0.05	0.17	0.01	0.05	0.01
669.5-2	M	543	29.13	20.11	18.67	1.83	18.09	0.39	0.02	0.05	0.04	0.02	0.04
239.8-3	M	211	29.49	18.95	18.66	1.94	18.59	0.43	0.03	0.05	—	0.02	0.13
239.8-4	M	211	29.00	19.62	18.75	1.66	18.81	0.41	0.01	0.01	0.01	—	—
239.8-5	M	211	29.14	19.79	18.67	1.88	18.29	0.40	0.04	—	0.01	0.02	0.01
754.6-1	M	623	30.25	18.82	17.70	2.65	18.05	0.66	0.05	0.14	—	—	0.21
754.6-3	M	623	29.89	19.27	18.63	2.13	17.74	0.72	0.06	0.05	0.01	0.01	—
754.6-4	M	623	29.96	18.59	18.38	2.18	18.14	0.69	0.05	0.06	—	0.06	0.02
636T2-1	M	511	31.00	18.88	18.03	3.48	15.96	0.70	0.02	0.08	0.02	0.03	0.02
636T2-3	M	511	30.30	19.47	18.68	2.45	16.55	0.77	0.03	0.07	0.01	0.32	0.04
636T2-4	M	511	29.21	19.97	18.78	1.82	17.26	0.83	0.11	0.02	—	0.18	0.03
636T2-5	M	511	29.47	19.71	19.38	2.00	16.61	0.82	0.09	0.06	—	0.02	—
553-1	M	436	27.71	20.16	19.58	0.73	17.71	1.70	—	0.05	0.04	—	1.06
553-2	M	436	28.11	21.07	18.20	1.49	17.70	1.64	0.01	0.03	—	—	0.05
553-3	M	436	28.15	19.66	19.08	0.60	18.69	2.13	0.06	0.01	0.04	0.01	0.21
553-5	M	436	27.75	21.01	20.52	0.40	18.17	0.99	0.04	0.01	0.01	0.02	0.03
553-6	M	436	27.35	21.98	18.63	1.26	17.45	1.18	0.11	—	—	0.02	—
293-1	M	235	28.63	18.61	17.49	1.36	21.01	0.81	0.11	0.01	—	0.02	0.03
819.5-1	M	684	29.85	18.88	17.36	2.32	18.78	0.81	0.01	0.08	0.03	0.24	0.05

(Continued on the following page)

TABLE 1 (Continued) Major elements of chlorite in the Naruo deposit.

Sample ID.	Type	Distance (m)	Major elements (%)										
			SiO ₂	Al ₂ O ₃	MgO	Fe ₂ O ₃	FeO	MnO	TiO ₂	CaO	Na ₂ O	K ₂ O	Cr ₂ O ₃
819.5-2	M	684	28.25	17.77	18.39	0.53	21.70	0.77	0.03	0.11	0.03	0.02	0.31
819.5-5	M	684	28.39	19.55	17.83	1.10	20.53	0.93	0.02	0.07	0.02	0.01	0.22
819.5-6	M	684	28.46	19.86	17.99	1.29	20.00	0.91	0.02	0.05	—	—	0.04
242.16-1	M	198	29.20	19.12	17.46	2.24	19.23	0.58	0.03	0.09	0.02	—	0.09
242.16-2	M	198	29.16	19.27	17.65	2.00	19.41	0.53	0.06	0.01	0.02	—	0.04
242.16-4	M	198	28.48	19.92	18.22	1.72	19.39	0.48	0.03	0.03	0.01	0.02	0.06
242.16-5	M	198	29.62	19.09	17.34	2.65	18.69	0.59	0.10	0.02	—	—	—
245.2-1	M	198	28.48	18.61	18.93	0.49	21.42	0.48	0.08	0.04	0.01	0.02	0.18
245.2-2	M	198	28.41	19.66	16.21	1.92	21.15	0.61	0.10	0.01	0.01	0.04	—
150.9-4	M	197	29.16	20.62	16.06	2.90	19.04	0.46	0.04	—	—	0.05	0.03
150.9-5	M	197	28.04	20.19	15.98	1.80	21.42	0.50	0.10	0.03	0.02	0.06	0.06
245.36-2	M	198	28.37	19.18	16.48	1.29	22.39	0.53	0.03	0.05	0.02	0.02	0.24
245.36-3	M	198	29.22	18.37	16.78	2.05	21.30	0.39	—	0.07	—	0.02	0.31
245.36-4	M	198	28.74	19.18	16.48	1.55	22.22	0.43	0.03	0.01	0.02	—	0.03
245.36-5	M	198	28.31	19.39	15.81	1.70	22.86	0.46	0.06	—	—	0.02	—
245.36-6	M	198	28.52	19.04	17.26	1.19	21.78	0.39	0.03	0.01	0.02	0.02	0.01
245.36-7	M	198	29.42	18.58	18.10	1.97	19.45	0.39	—	0.05	—	0.01	0.53
245.36-9	M	198	28.38	19.03	16.35	1.74	21.67	0.40	0.07	0.07	0.06	0.03	0.62
328.622	M	221	30.82	18.97	20.83	2.58	14.24	0.52	0.05	0.04	—	0.08	0.10
328.623	M	221	29.48	18.59	19.82	1.17	18.76	0.54	0.04	0.00	—	0.02	0.04
328.624	M	221	29.42	18.69	19.72	1.45	18.51	0.54	—	0.02	—	0.01	0.06
328-1	M	221	28.69	18.98	18.66	1.11	19.32	0.60	0.21	0.04	0.03	0.27	0.12
328-4	M	221	29.49	18.97	18.98	1.64	18.71	0.53	0.11	0.07	0.01	0.01	0.01
328-6	M	221	28.78	19.55	17.92	1.66	19.85	0.59	0.04	—	—	0.01	—
328-7	M	221	28.49	19.58	17.74	1.37	20.73	0.54	0.01	—	—	0.03	0.02
455.22-1	M	301	28.72	19.22	18.73	1.60	18.43	0.38	0.08	0.07	0.01	—	0.80
480.65-3	M	320	28.25	18.97	19.30	0.65	20.26	0.86	0.04	0.07	0.03	0.03	0.20
480.65-4	M	320	28.01	19.40	17.64	1.21	20.85	0.72	0.14	0.03	0.05	0.05	0.14
480.65-5	M	320	28.34	19.86	17.87	1.50	19.49	0.91	0.11	0.05	0.01	0.04	0.02
480.65-6	M	320	28.45	19.67	17.35	1.76	19.90	0.83	0.08	0.02	—	0.03	0.06
241.2-2	M	197	28.71	18.45	19.62	0.83	20.34	0.37	0.03	0.03	0.02	0.01	0.06
241.2-3	M	197	28.68	18.55	17.40	1.58	21.36	0.34	0.10	0.01	—	0.01	0.02

(Continued on the following page)

TABLE 1 (Continued) Major elements of chlorite in the Naruo deposit.

Sample ID.	Type	Distance (m)	Major elements (%)										
			SiO ₂	Al ₂ O ₃	MgO	Fe ₂ O ₃	FeO	MnO	TiO ₂	CaO	Na ₂ O	K ₂ O	Cr ₂ O ₃
241.2-4	M	197	28.19	19.16	18.82	0.74	20.29	0.37	0.05	0.08	0.03	—	0.20
78.8-3	M	76	27.71	19.92	18.78	0.29	21.03	0.73	—	0.04	0.11	0.01	0.08
78.8-4	M	76	28.55	20.08	17.47	1.66	19.75	0.44	0.02	—	0.01	0.15	0.05
78.8-5	M	76	29.19	18.66	17.91	1.86	20.22	0.27	—	0.03	0.02	—	0.02
453.4-1	M	1,010	27.17	20.91	14.71	1.52	23.18	0.92	0.03	0.02	—	—	0.02
453.4-2	M	1,010	28.07	21.19	14.22	2.32	21.16	0.89	0.01	0.03	0.06	0.34	0.06
453.4-5	M	1,010	26.79	20.16	16.05	0.38	24.09	0.81	0.03	—	0.03	0.01	0.14
444.7-1	M	1,008	27.90	20.63	15.64	1.80	21.21	0.78	0.08	0.08	0.05	—	0.25
591.1-3	M	1,043	28.91	19.44	16.22	2.03	20.32	0.94	0.08	0.08	0.04	0.03	0.08
591.1-5	M	1,043	28.67	18.91	17.42	1.28	21.06	0.73	0.02	—	0.03	—	0.04
591.1-6	M	1,043	28.11	19.45	18.75	0.62	20.68	0.95	0.07	0.03	—	—	0.07
376-1	M	221	27.56	19.95	16.36	1.44	20.40	1.03	0.03	0.03	0.03	0.09	1.20
376-2	M	221	28.12	20.16	17.00	1.42	20.34	1.00	—	0.01	0.02	0.03	0.04
376-3	M	221	27.86	19.50	18.85	0.33	20.80	0.95	0.04	0.03	—	0.05	0.06
376-4	M	221	27.85	20.27	16.84	1.31	20.64	1.00	0.05	0.01	0.03	0.01	0.04
376-5	M	221	28.22	20.07	17.05	1.71	19.90	1.04	0.09	—	—	0.01	—
376-9	M	221	28.21	20.05	16.44	1.45	20.98	0.99	0.04	0.10	0.08	0.02	0.19
376-1-	M	221	27.69	19.60	18.30	0.35	21.57	0.91	0.01	0.04	—	—	0.01
376-11	M	221	28.10	20.06	17.05	1.26	20.65	0.96	—	0.11	0.04	0.02	0.01
841.8	H	706	27.93	17.66	17.17	0.53	22.19	1.93	0.04	0.06	0.02	0.03	1.23
239.8-1	H	211	28.18	20.77	19.05	1.64	17.74	0.37	0.04	—	0.02	—	0.49
239.8-2	H	211	29.72	18.51	18.89	1.90	18.85	0.40	0.01	0.06	—	—	0.03
636T2-7	H	511	29.34	18.64	18.95	1.47	18.95	0.81	0.02	0.10	0.01	0.05	0.07
636T2-8	H	511	30.13	19.25	18.29	2.46	17.39	0.78	0.10	0.03	0.03	0.26	—
293-2	H	235	29.58	18.75	16.65	2.27	20.12	0.80	0.09	0.02	—	0.02	0.03
293-3	H	235	29.10	18.62	17.26	1.43	21.29	0.83	—	0.05	—	0.01	0.09
174.2-1	H	197	25.79	20.05	10.52	0.86	30.35	0.61	—	0.02	0.02	—	0.05
174.2-2	H	197	26.14	20.14	13.35	0.65	27.31	0.60	—	—	0.03	—	0.03
174.2-3	H	197	26.74	20.01	12.51	1.12	27.32	0.70	—	0.02	0.01	0.03	—
174.2-4	H	197	26.02	19.79	10.99	1.03	29.56	0.66	—	—	0.01	—	0.01
174.2-5	H	197	25.54	20.71	11.12	0.78	29.58	0.66	0.10	—	0.01	0.01	0.03
245.36-1	H	198	26.14	20.31	10.22	1.77	28.54	0.60	0.05	0.08	0.02	0.02	0.62

(Continued on the following page)

TABLE 1 (Continued) Major elements of chlorite in the Naruo deposit.

Sample ID.	Type	Distance (m)	Major elements (%)										
			SiO ₂	Al ₂ O ₃	MgO	Fe ₂ O ₃	FeO	MnO	TiO ₂	CaO	Na ₂ O	K ₂ O	Cr ₂ O ₃
359.85-1	H	237	25.57	21.37	10.47	1.35	28.27	1.14	0.07	—	—	—	0.09
359.85-2	H	237	26.71	20.76	10.32	2.46	26.82	0.88	0.15	—	—	—	0.02
359.85-3	H	237	24.93	21.43	9.98	0.99	29.68	1.09	0.09	—	0.01	—	0.03
359.85-4	H	237	28.18	20.72	9.32	3.70	25.15	0.91	—	0.03	0.07	0.04	0.18
359.85-5	H	237	27.34	20.84	7.96	3.31	28.21	0.50	0.05	0.09	0.01	—	0.05
359.85-6	H	237	25.98	21.24	11.71	1.29	26.99	1.18	0.10	—	0.04	—	0.04
359.85-7	H	237	25.88	20.91	8.04	1.90	29.31	2.19	—	0.05	0.05	0.01	0.25
78.8-1	H	76	28.20	20.12	17.96	1.28	20.27	0.54	0.02	—	0.03	—	—
382.2-1	H	1,000	28.17	18.16	19.17	0.00	21.42	1.09	—	0.07	0.08	0.07	0.44
382.2-2	H	1,000	27.91	21.19	15.55	2.05	20.59	1.33	0.07	0.01	0.02	—	0.02
382.2-3	H	1,000	27.91	20.88	15.43	1.95	20.60	1.32	0.05	0.02	0.02	0.01	0.03
382.2-4	H	1,000	27.69	20.65	16.06	1.26	21.77	1.20	—	—	0.04	0.02	0.10
382.2-5	H	1,000	27.76	20.80	15.70	1.67	20.95	1.45	—	—	0.03	0.03	0.04
382.2-6	H	1,000	26.09	20.56	10.69	1.14	28.40	1.69	0.02	0.04	0.05	0.01	0.06
453.4-3	H	1,010	25.40	21.12	9.56	1.05	29.65	2.09	0.05	—	0.02	—	—
453.4-4	H	1,010	25.71	21.07	10.17	1.37	27.85	1.91	—	0.01	0.02	—	0.03
453.4-6	H	1,010	28.13	20.60	16.07	1.68	21.31	0.93	0.02	0.02	0.01	0.02	0.06
257.9-1	H	994	29.22	20.17	18.40	2.21	17.15	0.96	0.04	0.01	0.03	0.03	0.04
444.7-4	H	1,008	28.29	20.30	16.24	1.79	20.42	0.94	0.02	0.13	0.02	0.03	0.24
444.7-6	H	1,008	28.16	20.17	16.12	1.85	20.42	1.06	0.02	0.03	0.05	0.02	0.43
444.7-7	H	1,008	28.26	20.49	16.62	1.66	20.33	1.12	0.02	—	0.03	—	—
591.1-1	H	1,043	27.68	20.51	16.03	1.60	21.17	1.29	—	0.05	0.03	0.03	0.14
376-6	H	221	26.92	20.68	13.91	1.55	23.63	1.17	0.02	0.02	0.05	0.03	0.27
376-7	H	221	26.69	21.22	14.50	1.21	23.03	1.33	—	—	0.05	—	0.29
376-8	H	221	26.96	21.00	15.51	1.07	22.28	1.25	—	—	0.04	0.03	—
343.9-1	H	189	27.57	21.42	15.15	1.91	20.97	1.29	0.05	0.04	0.03	—	0.16
343.9-2	H	189	27.25	20.91	16.04	1.11	22.13	0.96	0.02	—	0.02	—	0.04
343.9-3	H	189	27.68	20.99	15.60	1.69	21.37	0.80	—	0.02	0.03	0.01	—
343.9-5	H	189	25.77	20.89	11.93	1.27	25.50	1.55	0.05	0.04	0.10	0.01	1.29
343.9-6	H	189	26.85	21.38	14.56	1.34	23.41	1.11	0.02	0.06	0.01	0.03	0.01
343.9-7	H	189	27.78	21.14	15.18	1.81	22.02	0.87	0.06	0.05	—	—	0.03

(Continued on the following page)

TABLE 1 (Continued) Major elements of chlorite in the Naruo deposit.

Sample ID.	Type	Distance (m)	Major elements (%)										
			SiO ₂	Al ₂ O ₃	MgO	Fe ₂ O ₃	FeO	MnO	TiO ₂	CaO	Na ₂ O	K ₂ O	Cr ₂ O ₃
343.9-8	H	189	27.54	20.95	15.96	1.53	21.47	0.71	0.06	0.03	0.02	—	0.06
343.9-9	H	189	27.17	21.34	15.15	1.50	21.72	1.17	0.02	0.05	0.03	0.03	—

Fe₂O₃ contents are calculated using the ChloriteNorm table (Tindle, 2010) according to the principle that all cations occupy vacancies in the chlorite crystal structure. “/” means below the detection line.

TABLE 2 Atom number and important parameters of chlorite in Naruo deposit.

Sample ID.	Atom number of major elements (apfu)									Important parameters						
	Si	Al	Mn ³⁺	Fe ³⁺	Fe ²⁺	Mn	Ti	Mg	Cr	t (°C)	a ₃	a ₆	lga ₃	lga ₆	lgfO ₂	lgfS ₂
841.8-3	2.97	2.30	0.16	0.17	1.79	0.18	—	2.35	0.01	270	0.008	0.002	-2.1	-2.7	-39.2	-13.5
841.8-4	2.95	2.31	0.15	0.15	1.74	0.17	—	2.40	0.05	273	0.007	0.008	-2.1	-2.1	-38.0	-12.8
841.8-7	2.91	2.30	0.16	0.08	1.88	0.18	0.01	2.52	0.01	282	0.006	0.007	-2.2	-2.2	-37.7	-12.7
841.8-8	2.87	2.42	0.04	0.11	1.67	0.04	—	2.72	—	286	0.008	0.004	-2.1	-2.3	-38.1	-12.9
841.8-9	2.88	2.40	0.04	0.11	1.78	0.05	0.01	2.63	0.01	287	0.005	0.004	-2.3	-2.4	-37.0	-12.3
841.8-1	2.85	2.44	0.04	0.09	1.84	0.05	—	2.60	—	293	0.007	0.005	-2.2	-2.3	-37.2	-12.4
841.8-11	2.86	2.44	0.05	0.11	1.70	0.05	0.01	2.70	—	290	0.008	0.005	-2.1	-2.3	-37.0	-12.3
841.8-13	2.87	2.40	0.04	0.08	1.85	0.05	—	2.62	—	290	0.006	0.004	-2.3	-2.4	-36.9	-12.2
841.8-14	2.90	2.38	0.04	0.12	1.71	0.05	—	2.70	—	282	0.008	0.004	-2.1	-2.4	-37.4	-12.5
841.8-15	2.91	2.43	0.04	0.15	1.65	0.04	—	2.62	—	280	0.006	0.005	-2.3	-2.3	-37.6	-12.6
169.4-3	2.96	2.24	0.06	0.11	1.95	0.07	—	2.52	—	271	0.005	0.006	-2.3	-2.3	-37.4	-12.5
169.4-4	2.99	2.24	0.06	0.14	1.76	0.06	0.01	2.61	—	263	0.010	0.007	-2.0	-2.2	-39.0	-13.4
169.4-5	2.93	2.34	0.05	0.14	1.75	0.06	—	2.58	0.01	277	0.006	0.006	-2.2	-2.2	-39.5	-13.6
669.5-1	3.10	2.11	0.03	0.18	1.62	0.03	—	2.68	—	239	0.006	0.006	-2.2	-2.2	-37.8	-12.7
669.5-2	2.93	2.38	0.03	0.14	1.52	0.03	—	2.80	—	273	0.004	0.005	-2.4	-2.3	-41.9	-14.8
239.8-3	2.98	2.25	0.03	0.15	1.57	0.04	—	2.81	0.01	263	0.003	0.004	-2.5	-2.4	-38.0	-12.8
239.8-4	2.93	2.33	0.03	0.13	1.59	0.03	—	2.82	—	273	0.003	0.003	-2.5	-2.5	-36.2	-11.8
239.8-5	2.94	2.35	0.03	0.14	1.54	0.03	—	2.80	—	271	0.004	0.004	-2.5	-2.4	-39.9	-13.8
754.6-1	3.04	2.23	0.05	0.20	1.52	0.06	—	2.65	0.02	251	0.003	0.003	-2.6	-2.5	-37.9	-12.7
754.6-3	3.00	2.28	0.05	0.16	1.49	0.06	—	2.78	—	258	0.003	0.003	-2.5	-2.6	-36.6	-12.0
754.6-4	3.03	2.21	0.05	0.17	1.53	0.06	—	2.77	—	253	0.002	0.003	-2.6	-2.6	-36.2	-11.8
636T2-1	3.09	2.22	0.05	0.26	1.33	0.06	—	2.68	—	238	0.002	0.004	-2.7	-2.4	-37.7	-12.6
636T2-3	3.02	2.29	0.06	0.18	1.38	0.06	—	2.77	—	253	0.002	0.003	-2.7	-2.6	-37.1	-12.2

(Continued on the following page)

TABLE 2 (Continued) Atom number and important parameters of chlorite in Naruo deposit.

Sample ID.	Atom number of major elements (apfu)									Important parameters						
	Si	Al	Mn ³⁺	Fe ³⁺	Fe ²⁺	Mn	Ti	Mg	Cr	t (°C)	a ₃	a ₆	lga ₃	lga ₆	lgfO ₂	lgfS ₂
636T2-4	2.94	2.37	0.06	0.14	1.45	0.07	0.01	2.82	—	270	0.003	0.003	-2.6	-2.5	-38.9	-13.2
636T2-5	2.95	2.33	0.06	0.15	1.39	0.07	0.01	2.90	—	266	0.002	0.004	-2.7	-2.4	-41.0	-14.3
553-1	2.80	2.40	0.13	0.06	1.49	0.15	—	2.95	0.08	299	0.002	0.003	-2.7	-2.5	-39.8	-13.7
553-2	2.84	2.51	0.13	0.11	1.50	0.14	—	2.74	—	291	0.003	0.003	-2.6	-2.5	-38.3	-12.9
553-3	2.86	2.35	0.16	0.05	1.59	0.18	—	2.89	0.02	287	0.002	0.003	-2.7	-2.6	-38.6	-13.1
553-5	2.78	2.48	0.08	0.03	1.52	0.08	—	3.06	—	302	0.004	0.003	-2.4	-2.5	-39.6	-13.6
553-6	2.76	2.62	0.09	0.10	1.47	0.10	0.01	2.81	—	307	0.003	0.004	-2.6	-2.4	-39.7	-13.6
293-1	2.94	2.25	0.06	0.11	1.80	0.07	0.01	2.68	—	273	0.003	0.001	-2.6	-2.9	-36.6	-12.0
819.5-1	3.02	2.25	0.06	0.18	1.59	0.07	—	2.62	—	255	0.003	0.003	-2.5	-2.5	-36.2	-11.8
819.5-2	2.92	2.17	0.06	0.04	1.88	0.07	—	2.84	0.03	276	0.003	0.001	-2.5	-2.9	-38.2	-12.9
819.5-5	2.89	2.35	0.07	0.08	1.75	0.08	—	2.71	0.02	283	0.003	0.001	-2.5	-3.1	-37.5	-12.5
819.5-6	2.89	2.38	0.07	0.10	1.70	0.08	—	2.72	—	283	0.003	0.002	-2.5	-2.6	-34.9	-11.1
242.16-1	2.97	2.29	0.05	0.17	1.64	0.05	—	2.65	0.01	266	0.007	0.005	-2.2	-2.3	-38.7	-13.2
242.16-2	2.96	2.31	0.04	0.15	1.65	0.05	—	2.67	—	268	0.006	0.007	-2.2	-2.1	-39.6	-13.6
242.16-4	2.89	2.38	0.04	0.13	1.64	0.04	—	2.75	—	283	0.007	0.005	-2.2	-2.3	-39.3	-13.5
242.16-5	3.00	2.28	0.05	0.20	1.58	0.05	0.01	2.62	—	260	0.004	0.005	-2.4	-2.3	-39.7	-13.7
245.2-1	2.90	2.24	0.04	0.04	1.83	0.04	0.01	2.88	0.01	280	0.007	0.002	-2.2	-2.7	-40.2	-14.1
245.2-2	2.92	2.38	0.05	0.15	1.82	0.05	0.01	2.48	—	280	0.006	0.003	-2.2	-2.5	-38.0	-12.8
150.9-4	2.95	2.46	0.04	0.22	1.61	0.04	—	2.42	—	273	0.005	0.004	-2.3	-2.4	-37.7	-12.6
150.9-5	2.88	2.44	0.04	0.14	1.84	0.04	0.01	2.45	—	288	0.062	0.019	-1.2	-1.7	-35.1	-11.4
245.36-2	2.91	2.32	0.04	0.10	1.92	0.05	—	2.52	0.02	281	0.032	0.008	-1.5	-2.1	-35.8	-11.8
245.36-3	2.99	2.22	0.03	0.16	1.82	0.03	—	2.56	0.03	265	0.033	0.015	-1.5	-1.8	-35.9	-11.8
245.36-4	2.94	2.31	0.03	0.12	1.90	0.04	—	2.52	—	275	0.053	0.020	-1.3	-1.7	-35.3	-11.5
245.36-5	2.91	2.35	0.04	0.13	1.97	0.04	0.01	2.43	—	283	0.054	0.016	-1.3	-1.8	-34.4	-11.0
245.36-6	2.93	2.30	0.03	0.09	1.87	0.03	—	2.64	—	277	0.005	0.006	-2.3	-2.2	-38.7	-13.1
245.36-7	2.98	2.22	0.03	0.15	1.65	0.03	—	2.73	0.04	264	0.005	0.005	-2.3	-2.3	-38.7	-13.2
245.36-9	2.92	2.31	0.03	0.13	1.86	0.03	0.01	2.50	0.05	281	0.005	0.004	-2.3	-2.3	-37.3	-12.4
328.622	3.04	2.21	0.04	0.19	1.18	0.04	—	3.07	0.01	244	0.004	0.006	-2.4	-2.2	-39.1	-13.4
328.623	2.97	2.21	0.04	0.09	1.58	0.05	—	2.98	—	263	0.006	0.002	-2.2	-2.8	-39.9	-13.9
328.624	2.96	2.22	0.04	0.11	1.56	0.05	—	2.96	—	264	0.008	0.008	-2.1	-2.1	-37.5	-12.6

(Continued on the following page)

TABLE 2 (Continued) Atom number and important parameters of chlorite in Naruo deposit.

Sample ID.	Atom number of major elements (apfu)									Important parameters						
	Si	Al	Mn ³⁺	Fe ³⁺	Fe ²⁺	Mn	Ti	Mg	Cr	t (°C)	a ₃	a ₆	lga ₃	lga ₆	lgfO ₂	lgfS ₂
328-1	2.92	2.28	0.05	0.09	1.65	0.05	0.02	2.83	0.01	274	0.005	0.009	-2.3	-2.1	-37.4	-12.5
328-2	2.98	2.12	0.06	0.33	1.26	0.06	0.26	2.50	—	264	0.009	0.008	-2.1	-2.1	-36.7	-12.2
328-4	2.97	2.25	0.04	0.12	1.58	0.04	0.01	2.85	—	264	0.049	0.033	-1.3	-1.5	-34.1	-10.8
328-6	2.92	2.34	0.05	0.13	1.69	0.05	—	2.71	—	276	0.010	0.006	-2.0	-2.2	-38.2	-13.0
328-7	2.90	2.35	0.04	0.11	1.77	0.05	—	2.69	—	281	0.007	0.008	-2.1	-2.1	-39.2	-13.5
455.22-1	2.91	2.30	0.03	0.12	1.56	0.03	0.01	2.83	0.06	276	0.009	0.007	-2.0	-2.1	-38.5	-13.1
480.65-3	2.87	2.27	0.07	0.05	1.72	0.07	—	2.93	0.02	285	0.011	0.009	-1.9	-2.0	-37.6	-12.6
480.65-4	2.87	2.34	0.06	0.09	1.79	0.06	0.01	2.70	0.01	288	0.008	0.005	-2.1	-2.3	-38.7	-13.3
480.65-5	2.89	2.38	0.07	0.11	1.66	0.08	0.01	2.71	—	283	0.004	0.005	-2.4	-2.3	-39.2	-13.5
480.65-6	2.91	2.37	0.06	0.14	1.70	0.07	0.01	2.64	0.01	280	0.008	0.007	-2.1	-2.1	-37.7	-12.7
241.2-2	2.92	2.21	0.03	0.06	1.73	0.03	—	2.97	—	275	0.001	0.002	-3.1	-2.8	-40.6	-14.0
241.2-3	2.95	2.25	0.03	0.12	1.84	0.03	0.01	2.67	—	273	0.003	0.002	-2.5	-2.7	-40.1	-13.9
241.2-4	2.88	2.31	0.03	0.06	1.74	0.03	—	2.87	0.02	283	0.003	0.003	-2.5	-2.6	-39.6	-13.6
78.8-3	2.82	2.39	0.06	0.02	1.79	0.06	—	2.85	0.01	296	0.004	0.003	-2.4	-2.6	-38.9	-13.3
78.8-4	2.90	2.41	0.03	0.13	1.68	0.04	—	2.65	—	280	0.001	0.004	-2.9	-2.4	-37.2	-12.2
78.8-5	2.98	2.24	0.02	0.14	1.72	0.02	—	2.72	—	265	0.003	0.003	-2.5	-2.5	-39.2	-13.4
453.4-1	2.81	2.55	0.07	0.12	2.01	0.08	—	2.27	—	305	0.005	0.005	-2.3	-2.3	-38.0	-12.8
453.4-2	2.88	2.57	0.07	0.18	1.82	0.08	—	2.18	—	290	0.006	0.004	-2.2	-2.3	-37.8	-12.7
453.4-5	2.79	2.47	0.06	0.03	2.09	0.07	—	2.49	0.01	310	0.047	0.025	-1.3	-1.6	-33.1	-10.2
444.7-1	2.86	2.49	0.06	0.14	1.82	0.07	0.01	2.39	0.02	293	0.037	0.038	-1.4	-1.4	-34.1	-10.8
591.1-3	2.96	2.34	0.07	0.16	1.74	0.08	0.01	2.47	0.01	271	0.061	0.022	-1.2	-1.6	-32.7	-10.1
591.1-5	2.94	2.28	0.06	0.10	1.81	0.06	—	2.66	—	274	0.030	0.049	-1.5	-1.3	-36.0	-11.8
591.1-6	2.86	2.33	0.07	0.05	1.76	0.08	0.01	2.84	0.01	288	0.057	0.074	-1.2	-1.1	-34.9	-11.3
376-1	2.84	2.42	0.08	0.11	1.76	0.09	—	2.51	0.10	296	0.035	0.018	-1.5	-1.7	-33.8	-10.6
376-2	2.88	2.43	0.08	0.11	1.74	0.09	—	2.59	—	287	0.066	0.047	-1.2	-1.3	-33.2	-10.3
376-3	2.85	2.35	0.07	0.03	1.78	0.08	—	2.87	—	291	0.003	0.003	-2.5	-2.5	-37.8	-12.6
376-4	2.86	2.45	0.08	0.10	1.77	0.09	—	2.58	—	291	0.005	0.002	-2.3	-2.8	-38.4	-13.1
376-5	2.88	2.42	0.08	0.13	1.70	0.09	0.01	2.60	—	285	0.006	0.004	-2.2	-2.4	-37.2	-12.4
376-9	2.89	2.42	0.08	0.11	1.79	0.09	—	2.51	0.02	286	0.005	0.004	-2.3	-2.4	-37.1	-12.3
376-1-	2.84	2.37	0.07	0.03	1.85	0.08	—	2.80	—	294	0.005	0.005	-2.3	-2.3	-37.3	-12.4
376-11	2.88	2.42	0.07	0.10	1.77	0.08	—	2.60	—	287	0.005	0.002	-2.3	-2.7	-39.2	-13.5

(Continued on the following page)

TABLE 2 (Continued) Atom number and important parameters of chlorite in Naruo deposit.

Sample ID.	Atom number of major elements (apfu)									Important parameters						
	Si	Al	Mn ³⁺	Fe ³⁺	Fe ²⁺	Mn	Ti	Mg	Cr	t (°C)	a ₃	a ₆	lga ₃	lga ₆	lgfO ₂	lgfS ₂
841.8	2.89	2.16	0.15	0.04	1.92	0.17	—	2.65	0.10	284	0.007	0.006	-2.1	-2.2	-38.8	-13.2
239.8-1	2.84	2.46	0.03	0.12	1.49	0.03	—	2.86	0.04	292	0.005	0.002	-2.3	-2.7	-38.8	-13.3
239.8-2	3.00	2.20	0.03	0.14	1.59	0.03	—	2.84	—	258	0.006	0.004	-2.2	-2.4	-37.3	-12.4
636T2-7	2.97	2.22	0.06	0.11	1.60	0.07	—	2.86	0.01	264	0.006	0.001	-2.2	-3.0	-38.7	-13.3
636T2-8	3.02	2.27	0.06	0.19	1.46	0.07	0.01	2.73	—	255	0.005	0.005	-2.3	-2.3	-37.3	-12.5
293-2	3.01	2.25	0.06	0.17	1.71	0.07	0.01	2.53	—	259	0.005	0.005	-2.3	-2.3	-39.0	-13.3
174.2-1	2.78	2.55	0.05	0.07	2.74	0.06	—	1.69	—	322	0.007	0.008	-2.1	-2.1	-35.3	-11.4
174.2-2	2.77	2.52	0.05	0.05	2.42	0.05	—	2.11	—	318	0.008	0.008	-2.1	-2.1	-35.7	-11.6
174.2-3	2.83	2.50	0.06	0.09	2.42	0.06	—	1.97	—	307	0.009	0.006	-2.0	-2.2	-36.3	-11.9
174.2-4	2.80	2.51	0.05	0.08	2.66	0.06	—	1.77	—	317	0.008	0.007	-2.1	-2.1	-35.9	-11.7
174.2-5	2.74	2.62	0.05	0.06	2.65	0.06	0.01	1.78	—	331	0.046	0.020	-1.3	-1.7	-34.5	-11.0
245.36-1	2.80	2.56	0.05	0.14	2.56	0.05	—	1.63	0.05	319	0.014	0.010	-1.9	-2.0	-35.3	-11.4
359.85-1	2.74	2.69	0.09	0.11	2.53	0.10	0.01	1.67	0.01	332	0.010	0.012	-2.0	-1.9	-36.0	-11.8
359.85-2	2.84	2.60	0.07	0.20	2.38	0.08	0.01	1.64	—	310	0.061	0.024	-1.2	-1.6	-33.3	-10.4
359.85-3	2.69	2.73	0.09	0.08	2.68	0.10	0.01	1.61	—	342	0.046	0.025	-1.3	-1.6	-33.5	-10.5
359.85-4	2.96	2.57	0.07	0.29	2.21	0.08	—	1.46	0.02	285	0.014	0.003	-1.8	-2.6	-37.3	-12.6
359.85-5	2.91	2.62	0.04	0.27	2.51	0.04	—	1.26	—	299	0.008	0.007	-2.1	-2.1	-36.5	-12.0
359.85-6	2.75	2.65	0.10	0.10	2.39	0.11	0.01	1.85	—	325	0.003	0.004	-2.6	-2.4	-37.9	-12.7
359.85-7	2.80	2.66	0.18	0.15	2.65	0.20	—	1.29	0.02	324	0.009	0.008	-2.1	-2.1	-36.2	-11.8
78.8-1	2.87	2.41	0.04	0.10	1.72	0.05	—	2.72	—	288	0.007	0.007	-2.2	-2.2	-36.9	-12.2
382.2-1	2.89	2.19	0.08	—	1.84	0.09	—	2.93	0.04	283	0.007	0.007	-2.2	-2.2	-36.7	-12.1
382.2-2	2.85	2.55	0.10	0.16	1.76	0.11	0.01	2.36	—	296	0.007	0.006	-2.2	-2.2	-36.8	-12.2
382.2-3	2.86	2.52	0.10	0.15	1.77	0.11	—	2.36	—	292	0.008	0.007	-2.1	-2.2	-35.9	-11.7
382.2-4	2.84	2.49	0.09	0.10	1.86	0.10	—	2.45	0.01	298	0.007	0.007	-2.2	-2.1	-38.3	-13.0
382.2-5	2.85	2.52	0.11	0.13	1.80	0.13	—	2.40	—	295	0.007	0.005	-2.2	-2.3	-38.8	-13.3
382.2-6	2.78	2.59	0.14	0.09	2.54	0.15	—	1.70	—	321	0.006	0.002	-2.3	-2.7	-38.3	-13.1
453.4-3	2.73	2.68	0.17	0.08	2.67	0.19	—	1.53	—	335	0.007	0.005	-2.2	-2.3	-36.1	-11.8
453.4-4	2.76	2.67	0.16	0.11	2.50	0.17	—	1.63	—	326	0.006	0.005	-2.2	-2.3	-37.2	-12.4
453.4-6	2.87	2.48	0.07	0.13	1.82	0.08	—	2.44	—	291	0.006	0.001	-2.2	-3.0	-39.1	-13.5
257.9-1	2.94	2.39	0.07	0.17	1.44	0.08	—	2.76	—	271	0.007	0.005	-2.2	-2.3	-36.8	-12.2

(Continued on the following page)

TABLE 2 (Continued) Atom number and important parameters of chlorite in Naruo deposit.

Sample ID.	Atom number of major elements (apfu)									Important parameters						
	Si	Al	Mn ³⁺	Fe ³⁺	Fe ²⁺	Mn	Ti	Mg	Cr	t (°C)	a ₃	a ₆	lga ₃	lga ₆	lgfO ₂	lgfS ₂
444.7-4	2.89	2.44	0.07	0.14	1.74	0.08	—	2.47	0.02	286	0.006	0.005	-2.2	-2.3	-36.9	-12.2
444.7-6	2.88	2.43	0.08	0.14	1.75	0.09	—	2.46	0.04	287	0.016	0.012	-1.8	-1.9	-35.0	-11.2
444.7-7	2.88	2.46	0.09	0.13	1.73	0.10	—	2.52	—	287	0.014	0.008	-1.9	-2.1	-34.7	-11.1
591.1-1	2.84	2.48	0.10	0.12	1.82	0.11	—	2.45	0.01	296	0.011	0.006	-2.0	-2.2	-35.5	-11.5
376-6	2.81	2.54	0.09	0.12	2.06	0.10	—	2.17	0.02	307	0.008	0.006	-2.1	-2.2	-37.2	-12.4
376-7	2.77	2.60	0.11	0.09	2.00	0.12	—	2.25	0.02	314	0.007	0.001	-2.1	-2.9	-38.8	-13.4
376-8	2.79	2.56	0.10	0.08	1.93	0.11	—	2.40	—	308	0.007	0.005	-2.2	-2.3	-37.3	-12.4
343.9-1	2.82	2.59	0.10	0.15	1.80	0.11	—	2.31	0.01	301	0.009	0.009	-2.1	-2.1	-35.0	-11.2
343.9-2	2.80	2.54	0.07	0.09	1.90	0.08	—	2.46	—	305	0.010	0.006	-2.0	-2.2	-35.8	-11.7
343.9-3	2.84	2.54	0.06	0.13	1.84	0.07	—	2.39	—	297	0.009	0.008	-2.0	-2.1	-35.8	-11.7
343.9-5	2.73	2.61	0.12	0.10	2.26	0.14	—	1.89	0.11	328	0.026	0.014	-1.6	-1.8	-33.3	-10.3
343.9-6	2.78	2.61	0.09	0.10	2.03	0.10	—	2.25	—	313	0.015	0.009	-1.8	-2.0	-34.6	-11.0
343.9-7	2.84	2.55	0.07	0.14	1.88	0.08	—	2.31	—	298	0.011	0.010	-2.0	-2.0	-35.6	-11.5
343.9-8	2.83	2.53	0.06	0.12	1.84	0.06	—	2.44	—	300	0.009	0.007	-2.0	-2.2	-35.7	-11.6
343.9-9	2.80	2.60	0.09	0.12	1.87	0.10	—	2.33	—	306	0.010	0.008	-2.0	-2.1	-35.1	-11.3

MgO is distributed between 3% and 27%. Conversely, in Au, U, and Sn deposits, the FeO distribution primarily spans 20%–40%, with MgO ranging from 3% to 16%, indicating notable distinctions in their elemental compositions.

Earlier research has demonstrated that the concentrations of FeO and MgO in chlorite can be influenced by factors such as temperature, pressure, whole-rock composition, and fluid properties (Vidal et al., 2016). Li et al. (2022) discovered that chlorite in porphyry Cu-Mo-Au deposits, formed under various geological conditions, is primarily affected by the hydrothermal composition. The subsequent influencing factors included the composition of the surrounding rocks, whereas the impacts of pressure and temperature were nearly negligible. Intuitively, the fluid composition, encompassing various types of minerals, is likely a contributing factor to the FeO and MgO contents observed in the chlorite. Intuitively, the fluid composition, which encompasses various types of minerals, is likely a contributing factor to the magnesium (Mg) and iron (Fe) contents observed in the chlorite. However, as illustrated in Figure 5, the FeO and MgO contents of chlorite in porphyry Cu-polymetallic deposits exhibited notable differences when compared to those in granite-type U deposits, orogenic Au deposits, and skarn-type Sn deposits. Statistics reveal that the fluid temperature of porphyry Cu-polymetallic deposits ranges from 90°C to 957°C (Prokofiev et al., 2022), spanning high, medium, and low-temperature environments. In contrast, granite-type U deposits (80°C–440°C, Sassano et al., 1972),

orogenic Au deposits (220°C–450°C, Goldfarb et al., 2015) and skarn-type Sn polymetallic minerals (180°C–350°C, Bao et al., 2013) form in medium and low-temperature environments. The observed variation in the formation temperature closely aligns with the distribution ranges of the different mineral species, as depicted in Figure 5. Consequently, this study posits that one of the contributing factors to the distinct FeO and MgO contents in chlorite among the various mineral species is the variance in the ambient temperature during their formation. Investigating the potentially substantial impact of environmental pressure and the composition of the surrounding rock requires a more detailed examination. Principal component analysis (PCA) plays a crucial role in identifying the distinctive characteristics of the major elements in chlorite and identifying the various mineral species. Their significance extends to the potential analysis of trace elements and provides valuable insights for future research.

6.2 Geochemical characteristics of chlorite in Naruo deposit

6.2.1 Geochemical classification of chlorite

Chlorite can be divided into metasomatic-type (M-type) and hydrothermal vein-type (H-type) chlorite. However, the classification of the chemical composition is complicated owing

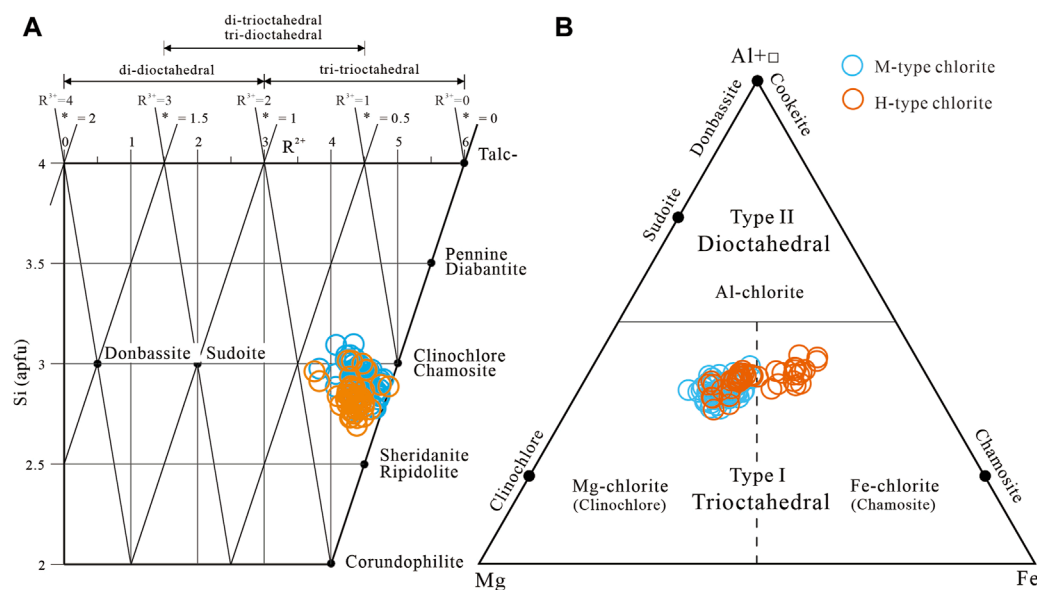


FIGURE 6
Classification diagram of the chemical composition of chlorite [(A) after Wiewióra and Weiss, 1990; (B) after Zane and Weiss, 1998].

to the complexity of the crystal structure. Previous studies have used the Si-TFe/(TFe+ Mg) classification method proposed by Hey (1954) to classify the chlorite in the Naruo deposit as mainly a diabase (Yang et al., 2015). However, this classification method failed to reflect the structural information of chlorite and was not genetically significant (Liu et al., 2016). In this study, the R^{2+} -Si (Wiewióra et al., 1990) and (Al+F2A5)-Mg-Fe (Zane et al., 1998) classification methods have become popular and useful in recent years. The R^{2+} -Si classification diagram shows that the M- and H-type of chlorites are located near the clinochlore and chamosite ranges and belong to the trioctahedral-trioctahedral structure (Figure 6A). Through the further division of the (Al+F2A5)-Mg-Fe three-terminal diagram, it can be clearly seen that there are differences in the chemical compositions of the M- and H-type chlorites. The results show that M-type chlorite is dominated by clinochlore, and all points fall into the Mg end-member area, whereas H-type chlorite includes clinochlore and chamosite, and points fall into the Mg and Fe end-member areas (Figure 6B). The formation of magnesium chlorite represents a low-oxygen fugacity and low-pH environment, whereas the formation of iron chlorite represents a relatively reduced environment (Inoue, 1995). Therefore, the M-type chlorite formed in the early stage was mainly formed in an environment of low oxygen fugacity and low pH value, whereas the H-type chlorite in the later stage had a large amount of iron chlorite, representing the reduced environment, indicating a reduced environment favourable for mineralisation.

6.2.2 Chlorite ion (cluster) replacement reaction

Chlorite formation is accompanied by three cation replacement modes: $\text{Fe}^{2+}=\text{Mg}$, Tschermak replacement, and dioctahedral-trioctahedral replacement (Bourdelle et al., 2013). Determining the

type of ion replacement reaction involved in chlorite formation in the Naruo deposit is useful for understanding the ion replacement rules and reflecting the physical and chemical circumstances of chlorite production. The diagram of the correlation among ions (clusters) of chlorite in the Naruo deposit shows that, overall, there is no 1:1 linear relationship between the Al^{IV} and Al^{VI} contents (Figure 7A), indicating that the ion replacement method of chlorite is not dominated by calcium–magnesium amphibole replacement but by other complex replacement methods (Xie et al., 1997).

The fundamental change in the alteration from clay and mica to chlorite is substituting aluminium for silicon (Hillier, 1993). The strong negative correlation between Al and Si (Figure 7B) verified this dominant alteration process. Al^{IV} and $\text{Fe}^{2+}/(\text{Fe}^{2+} + \text{Mg}^{2+})$ had a mild positive phase association (Figure 5C), demonstrating that when Al^{IV} and Si were substituted in the tetrahedral position, the absorption of Fe^{2+} and Mg^{2+} occurred in the octahedral position, causing Fe^{2+} to increase and Mg^{2+} to decrease. This assertion was supported by the negative relationship between Fe^{2+} and Mg^{2+} in Figure 5D. As Fe^{2+} replaces Mg^{2+} , more Al^{IV} is replaced by Si due to the modification of the chlorite structure (Xie et al., 1997). Consequently, the substitution of Fe^{2+} with Mg^{2+} promotes the development of chlorite alteration (Zhang et al., 2014). The higher Fe^{2+} content in the H-type chlorite (Figures 7B–D) suggests a more advanced state of chloritization alteration. The principal cations and Mg were shown to have a good linear connection after only one stage of chloritization alteration (Xie et al., 1997). However, the nonlinear relationship between Si, Al^{IV} , and Mg^{2+} (Figures 7E,F) in the chlorite in this study demonstrates that chloritization in the Naruo deposit was caused by a multitude of hydrothermal events rather than by a single metamorphism.

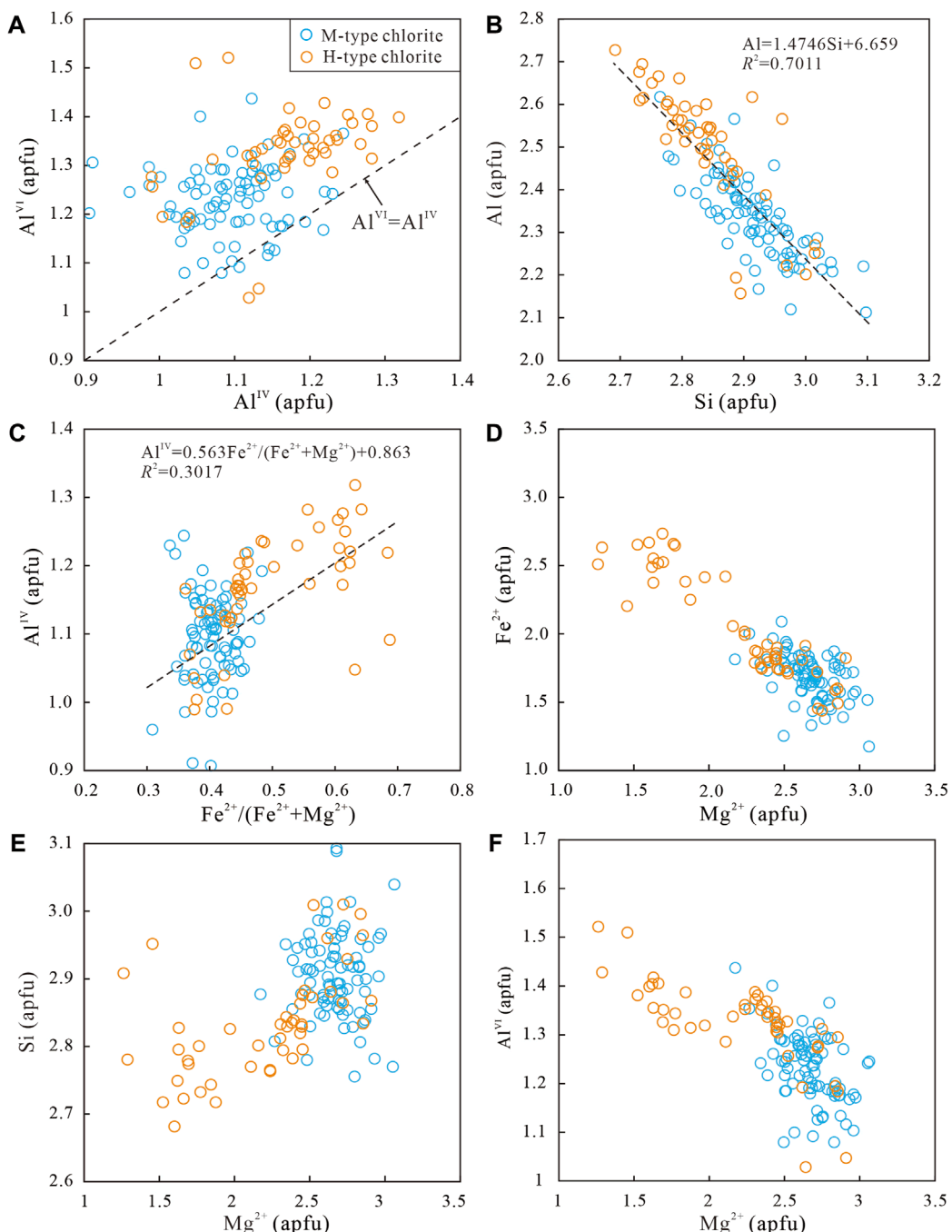


FIGURE 7
Binary diagram of Al^{VI} vs Al^{IV} (**A**), Al vs Si (**B**), Al^{IV} vs $\text{Fe}^{2+}/(\text{Fe}^{2+} + \text{Mg}^{2+})$ (**C**), Fe^{2+} vs Mg^{2+} (**D**), Si vs Mg^{2+} (**E**), and Al^{VI} vs Mg^{2+} (**F**) of chlorite in the Naruo deposit.

6.3 Formation environments and exploration indication of chlorite in Naruo deposit

6.3.1 Formation environments of chlorite

Geological thermometers are among the most frequently used tools for chlorite minerals in deposit research. The applicable conditions, advantages, and disadvantages of various

chlorite geothermometers and their development histories have been comprehensively summarised and introduced by previous researchers (Yavuz et al., 2015; Liu et al., 2016). Because substitution between Al, Fe, and Mg (Figure 7B) occurred during the formation of chlorite in the Naruo deposit, an empirical geothermometer involving Al^{IV} and $\text{Fe}^{2+}/(\text{Fe}^{2+} + \text{Mg}^{2+})$ content proposed by Kranidiotis and Maclean (1987) was chosen.

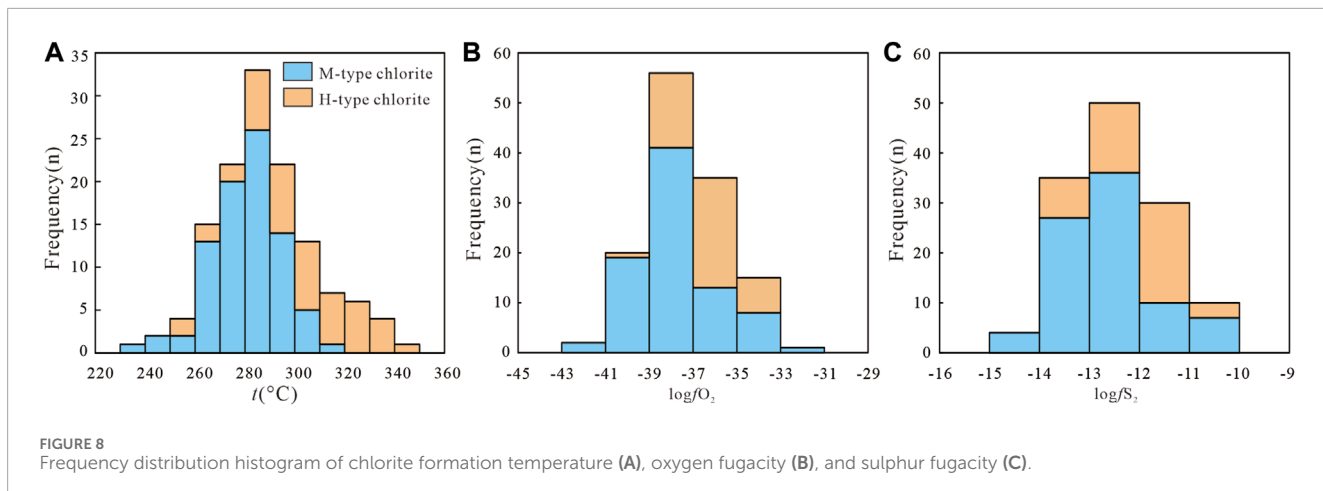


FIGURE 8
Frequency distribution histogram of chlorite formation temperature (A), oxygen fugacity (B), and sulphur fugacity (C).

$$t(\text{°C}) = 212 \times \left(\text{Al}^{\text{IV}} + 0.35 \times \frac{\text{Fe}}{\text{Fe} + \text{Mg}} \right) + 18 \quad (1)$$

The calculated results (Table 2) show that the chlorite formation temperature of the Nara deposit is between 255°C and 342°C (Figure 6A) with an average value of 286°C. The above temperature falls within the 200°C–350°C range for fluid inclusion homogenisation during the chloritization stage (Sun et al., 2015). Given the intimate association between chlorite and the development of chalcopyrite, the geological temperature of chlorite (238°C–342°C) suggested that the Naruo deposit's Cu mineralisation occurred primarily in a medium-temperature environment. Among them, M-type chlorite is formed at 238°C–310°C (average value of 277°C), which is generally lower than the formation temperature of H-type chlorite at 255°C–342°C (average value of 301°C) (Figure 8A). Chloritization alteration generally occurs during the cooling process after the emplacement of high-temperature magmatic melts (Yang et al., 2005; Yang et al., 2008; Hou et al., 2009; Sillitoe et al., 2010). The phenomenon of increasing H-type chlorite formation temperature in the Naruo deposit implies the presence of multistage magmatic-hydrothermal activity, which agrees with the conclusion that chloritization of the Naruo deposit does not occur in a single metamorphism.

Since Walshe (1986) proposed a six-component solid-solution model of chlorite, it has become possible to calculate the oxygen and sulphur fugacities of chlorite, and this method has been widely used (Xiao et al., 1993; Zheng et al., 1997; Zhang et al., 2014; Zhang et al., 2020). In this work, it was discovered that the Naruo deposit has a mineral combination of chlorite+quartz+Al₂SiO₅ (aluminosilicate mineral) ± oxide ± sulphide; therefore, the oxygen and sulphur fugacity of chlorite may be calculated using the six-component solid solution model (Walshe, 1986). Please refer to Walshe (1986) for the calculation method. The calculation method involving the equilibrium constant adopts the formula modified by Zhang et al. (2014).

$$\log K_1 = 21.77 \times e^{-0.003t} \quad (2)$$

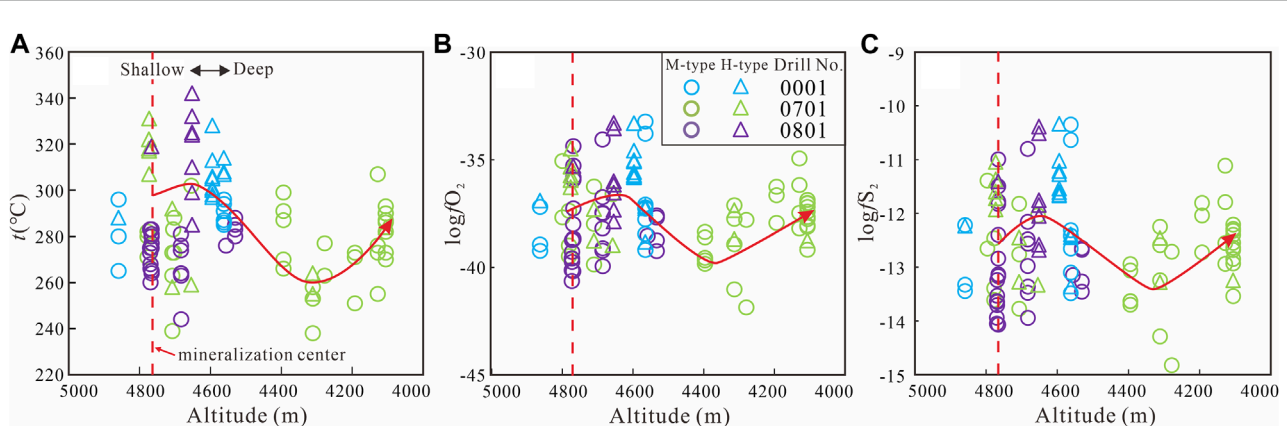
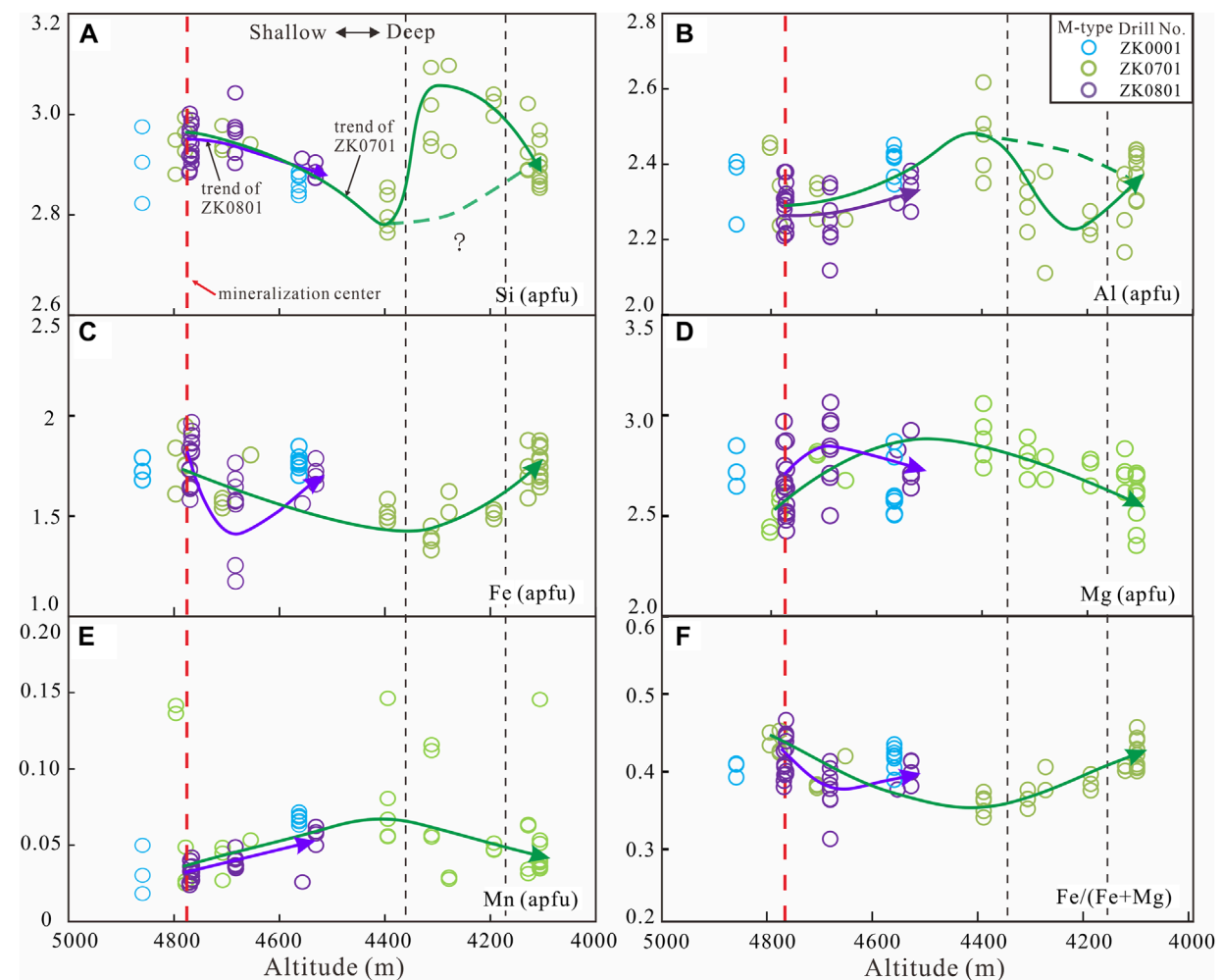
$$\log K_2 = 0.1368t - 0.0002t^2 - 82.615 \quad (3)$$

The oxygen fugacity of chlorite ranges between -49.6 and -32.7, with an average of -37.3. The M-type chlorite (-41.9–32.7) and H-type chlorite (-39.1–33.3) in the Naruo deposit have similar lgfO₂ value ranges (Figure 6B). The sulphur fugacity lgfS₂ value of chlorite is between -14.8 and -10.1. The two types of chlorites have similar sulphur fugacity values: lgfS₂ (M-type) = -14.8–10.1, lgfS₂ (H-type) = -13.5–10.3 (Figure 8C). The precipitation of Cu sulphide indicates the progressive transition of the ore-bearing hydrothermal fluid environment from oxidation to reduction (Sillitoe et al., 2010; Li et al., 2006; Hou et al., 2020), resulting in lower oxygen and sulphur fugacities in the environment. However, the oxygen and sulphur fugacities of the late H-type chlorite did not vary appreciably (Figures 8B,C), confirming that several magmatic-hydrothermal processes influenced the mineralisation of the Naruo deposit.

6.3.2 Prospecting and exploration indication of chlorite

The chemical elements of chlorite in porphyry Cu deposits exhibit specific spatial changes (Wilkinson et al., 2015; Cooke et al., 2020; Fan et al., 2021). For example, the chemical composition of chlorite in Indonesia's Batu Hijau porphyry Cu deposit shows systematic changes from the hydrothermal mineralisation centre to the edge of the deposit, especially within a radius of 2.5 km from the mineralisation centre (Wilkinson et al., 2015). This has also been verified in a resolution porphyry deposit in the United States, and the hydrothermal mineralisation centre was successfully found in the blind area (Cooke et al., 2020). Consequently, the alteration of chlorite chemical components is becoming increasingly popular in the prospecting and investigation of porphyry deposits, although Xiao et al. (2020a, b) proposed that using elements such as Fe, Mg, Co, and Ni as geochemical vectors might not be appropriate. Previous studies have revealed a significant positive correlation between the chlorite Al^{IV}, Fe²⁺/(Fe²⁺+Mg²⁺), and Cr/Ti ratios within the porphyry body and the ore grades of Cu and Au, serving as indicative markers for locating enriched ore bodies within porphyry-type deposits (Yang et al., 2015).

To mitigate the influence of multiphase hydrothermal activities on chlorite composition and considering the heightened sensitivity and mobility of H-type chlorite, we chose the elevation of M-type chlorite samples within the magmatic metallogenetic system



(ZK0001, ZK0701, and ZK0801) as the abscissa. This selection enabled us to observe the chemical indicators of chlorite in ore prospecting, particularly considering the pronounced sensitivity of H-type chlorite to external environmental factors. According to the Cu grade and AA' profile (Figure 2), an altitude of 4784 m (red dotted line) is the most Cu-rich mineralisation centre (Figure 9). As shown in Figure 7, some chlorite chemical components follow specific patterns as they progress from the shallow mineralisation centre to the deep intrusions. The contents of Si, Fe, and the ratio of Fe/(Fe+Mg) in the main elements of chlorite gradually decrease but increase with depth. In contrast, the Al, Mg, and Mn content gradually increased and then decreased with depth. In particular, Si and Al showed different trends from the other elements at an altitude of 4,300 m (Figures 9A,B).

Xiao et al., 2020a, b) proposed that in the process of chloritization of the mafic minerals in the Xiaokelehe and Atlas porphyry Cu deposits, the contents of the major elements Fe, Mg, and Mn are greatly affected by the composition and type of the precursor minerals, whereas the contents of elements such as Al and Ti can be used as a reflection of the hydrothermal characteristics. Therefore, we believe that the Al and Si elements of the Naruo metasomatic-type chlorite may have originated primarily from hydrothermal fluid, making them more sensitive and reflecting more information about hydrothermal characteristics. In contrast, Fe, Mg, Mn, and other elements were significantly influenced by the type and composition of the precursor minerals and reflected less on the hydrothermal composition; therefore, they only exhibited a single change trend (Figures 9C–F). As a result, we believe there might be another hydrothermal mineralisation centre deep in the Naruo porphyry system, but it is still necessary to strengthen the mineralogy and trace element research of chlorite to determine the location of another mineralisation centre and properly direct upcoming prospecting work.

In addition, the continuous precipitation of metal sulphides also reduces oxygen and sulphur fugacity as the ore-forming system cools, atmospheric water is added, and other factors (Richards et al., 1993; 1995). In contrast, the temperature, oxygen fugacity, and sulphur fugacity of the late H-type chlorite are significantly higher than those of the early M-type chlorite (Figure 10), indicating the addition of magmatic-hydrothermal fluid at a later stage. Among the contemporaneous chlorites, the oxygen and sulphur fugacity values of the proximal chlorite near the mineralisation centre were higher than those of the distal chlorite, which is compatible with the properties of the fluid in the magma dissolving centre. The chlorite temperature, oxygen fugacity, and sulphur fugacity values demonstrated a pattern of decreasing and then increasing from the shallow mineralisation centre to the deep intrusion, suggesting that the second stage of hydrothermal mineralisation may have occurred from the deep.

7 Conclusion

- (1) The principal component analysis method was proven to be effective in distinguishing two distinctive element signatures within chlorite and categorising them into four deposit types. These types include orogenic Au deposits, granite-type U deposits, and skarn-type Sn polymetallic deposits, which are

characterised by high FeO and low MgO contents, separating them from porphyry Cu deposits. These distinctions can be attributed to temperature and fluid composition variations during their formation.

- (2) Clinochlore (Mg end-member) and chamosite (Fe end-member) are two subgroups of the Naruo chlorite distinguished by their chemical components. Metasomatic (M-type) chlorite is entirely composed of Mg chlorite, indicating a low oxygen fugacity and pH value; hydrothermal (H-type) chlorite is a mixture of Mg and Fe chlorites, representing a reduced environment conducive to mineralisation.
- (3) The chlorite in the Naruo deposit is generated primarily in a medium-temperature environment (255°C–342 °C). Late H-type chlorite has a higher formation temperature and oxygen and sulphur fugacities, similar to those of M-type chlorite, indicating the presence of multiple magmatic-hydrothermal events.
- (4) From the mineralisation centre to the periphery, the contents of Si and Fe and the Fe/(Fe+Mg) ratio in M-type chlorite gradually decreased, whereas those of Al, Mg, and Mn in M-type chlorite gradually increased. Temperature, sulphur, and oxygen fugacity in all chlorites decreased. Using the above indicators, it can be predicted that there may be a large prospecting potential in the deep regions. (Xiao et al., 2018a; Wangm et al., 2018).

Data availability statement

Publicly available datasets were analyzed in this study. This data can be found here: The original data for this article has already been inserted into the text, while a significant amount of additional data has been extracted from publicly published articles, with proper references provided in this paper.

Author contributions

FL: Data curation, Investigation, Writing—original draft, Writing—review and editing. JT: Funding acquisition, Project administration, Supervision, Writing—review and editing. YS: Methodology, Project administration, Resources, Supervision, Writing—review and editing. SL: Investigation, Resources, Writing—review and editing. PT: Data curation, Formal Analysis, Investigation, Methodology, Software, Writing—original draft, Writing—review and editing. HaL: Investigation, Methodology, Resources, Writing—review and editing, Writing—original draft. HY: Data curation, Formal Analysis, Investigation, Software, Writing—review and editing. QW: Data curation, Investigation, Methodology, Resources, Software, Writing—review and editing. YW: Data curation, Formal Analysis, Investigation, Writing—original draft. ZD: Data curation, Formal Analysis, Investigation, Methodology, Writing—review and editing. YL: Investigation, Methodology, Resources, Writing—review and editing. JL: Investigation, Methodology, Resources, Writing—review and editing. Hol: Investigation, Methodology, Resources, Writing—review and editing. YD: Investigation, Methodology, Resources, Writing—review and editing.

Funding

The author(s) declare financial support was received for the research, authorship, and/or publication of this article. This research was funded by the national key research and development program of China, grant number 2022YFC2905001; the basic research fund of Chinese academy of geological sciences, grant number JKYZD202316; the national natural science foundation of China, grant number 42230813, 42172100; and the fund from Sinoprobe Laboratory, Chinese Academy of Geological Sciences, grant number SL202405.

Acknowledgments

We are deeply grateful to the reviewers for their constructive comments that improved the manuscript greatly. We thank all editors for their efficient handling on this manuscript.

References

- Bai, R. (2016). Geochemical characteristics and genesis of magmatic rocks for Duolong ore concentrated area in Tibet. master's thesis.
- Bao, T., and Ye, L. (2013). Study on the ore-forming fluids of Dulong skarn-type tin-zinc polymetallic deposit. *Acta Mineral. Sin.* 33, 426–427. doi:10.16461/j.cnki.1000-4734.2013.s2.332
- Battaglia, S. (1999). Applying X-ray geothermometer diffraction to a chlorite. *Clay Clay Min.* 47, 54–63. doi:10.1346/CCMN.1999.0470106
- Bourdelle, F. (2021). Low-temperature chlorite geothermometry and related recent analytical advances: a review. *Minerals-Basel* 11, 130. doi:10.3390/min11020130
- Bourdelle, F., Parra, T., Chopin, C., and Beyssac, O. (2013). A new chlorite geothermometer for diagenetic to low grade metamorphic conditions. *Contrib. Mineral. Petr.* 165, 723–735. doi:10.1007/s00410-012-0832-7
- Cathelineau, M. (1988). Cation site occupancy in chlorites and illites as a function of temperature. *Clay Min.* 23, 471–485. doi:10.1180/claymin.1988.023.4.13
- Cathelineau, M., and Nieve, D. (1985). A chlorite solid solution geothermometer for the Los Azufres (Mexico) geothermal system. *Contrib. Mineral. Petr.* 91, 235–244. doi:10.1007/BF00413350
- Chang, Z., Hedenquist, J. W., White, N. C., Cooke, D. R., Roach, M., Deyell, C. L., et al. (2011). Exploration tools for linked porphyry and epithermal deposits: example from the mankayan intrusion-centered Cu-Au district, luzon, Philippines. *Econ. Geol.* 106, 1365–1398. doi:10.2113/econgeo.106.8.1365
- Cooke, D. R., Wilkinson, J. J., Baker, M., Agnew, P., Phillips, J., Chang, Z., et al. (2020). Using mineral chemistry to aid exploration; a case study from the Resolution porphyry Cu; Mo deposit, Arizona. *Econ. Geol. Bull. Soc. Econ. Geol.* 115, 813–840. doi:10.5382/econgeo.4735
- De Caritat, P., Hutcheon, I., and Walshe, J. L. (1993). Chlorite geothermometry; a review. *Clay Clay Min.* 41, 219–239. doi:10.1346/CCMN.1993.0410210
- Deer, D. W., Howie, R. A., and Zussman, J. (1963). *Rock-forming minerals: sheet silicates*. London: Longmans.
- Ding, S. (2014). master's thesis. Chengdu: Chengdu University of Technology. The study of geological characteristics of Naruo copper (gold) deposit in gaize, Tibet
- Ding, S., Chen, Y. C., Tang, J. X., Zheng, W. B., Lin, B., and Yang, C. (2017). Petrogenesis and Tectonics of the Naruo porphyry Cu(Au) deposit related intrusion in the Duolong area, central Tibet. *Acta Geol. Sin. - Engl. Ed.* 91, 581–601. doi:10.1111/1755-6724.13119
- Fan, Y., Zhang, W., Liu, Y., Zhou, T., Zhang, L., Chen, X., et al. (2021). Geochemical characteristics of chlorite in the Luohe iron deposit in the middle-lower Yangtze metallogenic Belt, Eastern China. *Ore Geol. Rev.* 133, 104062. doi:10.1016/j.oregeorev.2021.104062
- Feng, Y., Chu, G., Xiao, B., Li, R., Deng, C., Li, G., et al. (2022). Chlorite mineralogy, geochemistry and exploration implications: a case study of the Xiaokelehe porphyry Cu-Mo deposit in NE China. *Ore Geol. Rev.* 140, 104568. doi:10.1016/j.oregeorev.2021.104568
- Foster, M. D. (1962). *Interpretation of the composition and a classification of the chlorites*. U.S. Geological Survey Professional Papers, U.S.Govt. Print. Off., A1–A33. doi:10.3133/pp414A
- Gao, K., Duo, J., Tang, J., Zhang, Z., Song, J., Ding, S., et al. (2016). Alteration of Naruo porphyry Cu (Au) deposit in the Duolong ore-concentration area, Tibet. *Bull. Mineralogy, Petrology Geochem.* 35 (6), 1226–1237. (in Chinese with English abstract). doi:10.3969/j.issn.1007-2802.2016.06.013
- Gao, K., Song, Y., Liu, Z., Yang, H., and Wang, Y. (2021). Sulfur and lead isotope composition and tracing for sources of ore-forming materials in the Naruo Cu (Au) deposit, in Tibet. *Sediment. Geol. Tethyan Geol.*, 1–12. (in Chinese with English abstract). doi:10.19826/j.cnki.1009-3850.2021.05002
- Gao, K., Tang, J., Song, Y., Liu, Z., Fang, X., Yang, H., et al. (2017). Genesis of magmatic rocks of cryptoe-plosive breccia in the Naruo deposit of Tibet: evidence from zircon Hf isotope. *Geol. Explor.* 53 (2), 0207–0216. (in Chinese with English abstract). doi:10.13712/j.cnki.dzykt.2017.02.001
- Goldfarb, R. J., and Groves, D. I. (2015). Orogenic gold: common or evolving fluid and metal sources through time. *Lithos* 233, 2–26. doi:10.1016/j.lithos.2015.07.011
- Hey, M. H. (1954). A new review of the chlorites. *Mineralogical Mag. J. Mineralogical Soc.* 30, 277–292. doi:10.1180/minmag.1954.030.224.01
- Hillier, S. (1993). Origin, diagenesis, and mineralogy of chlorite minerals in devonian lacustrine mudrocks, orcadian basin, scotland. *Clay Clay Min.* 41, 240–259. doi:10.1346/CCMN.1993.0410211
- Hou, Z., and Yang, Z. (2009). Porphyry deposits in continental settings of China: geological characteristics, magmatic hydrothermal system, and metallogenic model. *Acta Geol. Sin.* 83 (12), 1779–1817. (in Chinese with English abstract).
- Hou, Z., Yang, Z., Wang, R., and Zheng, Y. (2020). Further discussion on porphyry Cu-Mo-Au deposit formation in Chinese mainland. *Earth Sci. Front.* 27 (02), 20–44. (in Chinese with English abstract). doi:10.13745/j.esf.2020.3
- Hu, B., Zeng, L., Liao, W., Wen, G., Hu, H., Li, M. Y. H., et al. (2022). The origin and discrimination of high-Ti magnetite in magmat-ic-hydrothermal systems: insight from machine learning analysis. *Econ. Geol.* 117, 1613–1627. doi:10.5382/econgeo.4946
- Inoue, A. (1995). “Formation of clay minerals in hydrothermal environments,” in *Origin and mineralogy of clays: clays and the environment*. Editor B. Velde (Berlin, Heidelberg: Springer Berlin Heidelberg), 268–329.
- Inoue, A., Kurokawa, K., and Hatta, T. (2010). Application of chlorite geothermometry to hydrothermal alteration in toyohira geothermal system, southwestern hokkaido, Japan. *Resour. Geol.* 60, 52–70. doi:10.1111/j.1751-3928.2010.00114.x
- Inoue, A., Meunier, A., Patrier-Mas, P., Rigault, C., Beaufort, D., and Vieillard, P. (2009). Application of chemical geothermometry to low-temperature trioctahedral chlorites. *Clay Clay Min.* 57, 371–382. doi:10.1346/CCMN.2009.0570309
- Jolliffe, I. T. (2002). *Principal component analysis for special types of data*. New York: Springer.

Conflict of interest

Author SL was employed by Golden Dragon Mining Co., Ltd. Author HaL was employed by China 19th Metallurgical Corporation.

The remaining authors declare that the research was conducted in the absence of any commercial or financial relationships that could be construed as a potential conflict of interest.

Publisher's note

All claims expressed in this article are solely those of the authors and do not necessarily represent those of their affiliated organizations, or those of the publisher, the editors and the reviewers. Any product that may be evaluated in this article, or claim that may be made by its manufacturer, is not guaranteed or endorsed by the publisher.

- Kranidiotis, P., and MacLean, W. H. (1987). Systematics of chlorite alteration at the Phelps Dodge massive sulfide deposit, Matagami, Quebec. *Econ. Geol.* 82, 1898–1911. doi:10.2113/gsecongeo.82.7.1898
- Li, C. (1987). The Longmucuo–Shuanghu–Lancangjiang plate suture and the north boundary of distribution of Gondwana facies Permo-Carboniferous system in northern Xizang, China. *Journal of Jilin University: Earth Science Edition* 17, 155–166.
- Li, C., Shen, P., Zhao, Y., Li, P., Zhang, L., and Pan, H. (2022a). Mineral chemistry of chlorite in different geologic environments and its implications for porphyry Cu ± Au ± Mo deposits. *Ore Geol. Rev.* 149, 105112. doi:10.1016/j.oregeorev.2022.105112
- Li, F. (2022). *Metallogenetic mechanism of Naruo large porphyry Cu (Au) deposit in Tibet: evidences from mineralogy*. Beijing: China University of Geosciences doctoral thesis.
- Li, F., Tang, J., Zhang, J., Song, Y., Li, H., Lin, B., et al. (2022b). Discovery of Late Early Cretaceous diorite porphyry from the Shamuluo formation in the Gaize area, Tibet: response to the northward subduction plate rollback event of Bangongco–Nujiang Tethys Ocean. *Acta Petrol. Sin.* 38 (1), 185–208. (in Chinese with English abstract). doi:10.18654/1000-0569/2022.01.13
- Li, J., Li, G., Qin, K., and Xiao, B. (2008). Geochemistry of porphyries and volcanic rocks and ore-forming geochronology of Duobuza gold-rich porphyry copper deposit in Bangonghu belt, Tibet, Constraints on metallogenic tectonic settings. *Acta Petrol. Sin.* 24, 531–543. (in Chinese with English abstract).
- Li, J., Qin, K., Li, G., Xiao, B., Zhao, J., and Chen, L. (2016). Petrogenesis of Cretaceous igneous rocks from the Duolong porphyry Cu-Au deposit, central Tibet: evidence from zircon U-Pb geochronology, petrochemistry and Sr-Nd-Pb-Hf isotope characteristics. *Geol. J.* 51, 285–307. doi:10.1002/gj.2631
- Li, J., Q. K., and Li, G. (2006). Basic characteristics of gold-rich porphyry copper deposits and their ore sources and evolving processes of high oxidation magma and ore-forming fluid. *Acta Petrol. Sin.* 22 (3), 678–688. (in Chinese with English abstract).
- Li, Y. (2021). Geochemistry of chlorite from north Zegulang ore segment in the Jiamu deposit, Tibet. Beijing: China University of Geosciences. master's thesis.
- Liao, Z., Liu, Y., Li, C., Ye, L., Liu, S., and Zheng, W. (2010). Characteristics of chlorites from Dulong Sn -Zn deposit and their metallogenic implications. *Miner. Deposits* 29 (1), 169–176. (in Chinese with English abstract). doi:10.16111/j.0258-7106.2010.01.018
- Lin, B., Fang, X., Wang, Y., Yang, H., and He, W. (2019a). Petrologic genesis of ore-bearing porphyries in Tiegelongnan giant Cu (Au, Ag) deposit, Tibet and its implications for the dynamic of Cretaceous mineralization, Dulong. *Acta Petrol. Sin.* 35 (03), 642–664. (in Chinese with English abstract). doi:10.18654/1000-0569/2019.03.03
- Lin, B., Tang, J., Chen, Y., Song, Y., Hall, G., Wang, Q., et al. (2017). Geochronology and genesis of the tiegelongnan porphyry Cu(Au) deposit in Tibet: evidence from U-Pb, Re-Os dating and Hf, S, and H-O isotopes. *Resour. Geol.* 67, 1–21. doi:10.1111/rge.12113
- Lin, B., Tang, J., Tang, P., Georges, B., Crystal, L., Li, F., et al. (2024). MULTIPULSED MAGMATISM AND DURATION OF THE HYDROTHERMAL SYSTEM OF THE GIANT JIAMA PORPHYRY Cu SYSTEM, TIBET, CHINA. *Econ. Geol.* 119 (01), 201–217. doi:10.5382/econgeo.5054
- Lin, B., Tang, J. X., Chen, Y. C., Baker, M., Song, Y., Yang, H. H., et al. (2019b). Geology and geochronology of Naruo large porphyry-breccia Cu deposit in the Duolong district, Tibet. *Gondwana Res.* 66, 168–182. doi:10.1016/j.gr.2018.07.009
- Liu, S., Liu, Y., Ye, L., Wei, C., Chen, W., and Hu, Y. (2022). Genetic mineralogy of chlorite in the dulong Sn-Zn polymetallic deposit in maguan, yunnan province, China. *Acta Mineral. Sin.* 42 (1), 1–13. (in Chinese with English abstract). doi:10.16461/j.cnki.1000-4734.2021.41.091
- Liu, Y., Zhang, S., and Zhang, H. (2016). Advances on mineral genesis of chlorite: a review. *Adv. Geosciences* 6 (3), 264–282. (in Chinese with English abstract). doi:10.12677/ag.2016.63028
- Pacey, A., Wilkinson, J. J., and Cooke, D. R. (2020). Chlorite and epidote mineral chemistry in porphyry ore systems: a case study of the northparkes district, new south wales, Australia. *Econ. Geol.* 115, 701–727. doi:10.5382/econgeo.4700
- Pan, G. T., Wang, L. Q., Li, R. S., Yuan, S. H., Ji, W. H., Yin, F. G., et al. (2012). Tectonic evolution of the Qinghai-Tibet plateau. *J. Asian Earth Sci.* 53, 3–14. doi:10.1016/j.jseaes.2011.12.018
- Prokofiev, V. Y., and Naumov, V. B. (2022). Ranges of physical parameters and geochemical features of mineralizing fluids at porphyry de-positions of various types of the Cu-Mo-Au system: evidence from fluid inclusions data. *Minerals-Basel* 529, 529. doi:10.3390/min12050529
- Qin, L., Liu, X., Wang, K., Zhang, Z., Peng, Y., Wellington, D., et al. (2018). High level antibody response to pandemic influenza H1N1/09 virus is associated with interferon-induced transmembrane protein-3 rs12252-CC in young adults. *East China Geol.* 39 (2), 134–141. (in Chinese with English abstract). doi:10.3389/fcimb.2018.00134
- Richards, J. P. (1995). “Alkalic-type epithermal gold deposits—a review,” in *Magmas, fluids, and ore deposits*, Editor J. E. H. Thompson (Mineralogical Association of Canada), 367–400. Short Course Series 23.
- Richards, J. P., and Kerrich, R. (1993). The Porgera gold mine, Papua New Guinea; magmatic hydrothermal to epithermal evolution of an alkal-ic-type precious metal deposit. *Econ. Geol. Bull. Soc. Econ. Geologists* 88, 1017E–1052E. doi:10.2113/gsecongeo.88.5.1017
- Sassano, G. P., Fritz, P., and Morton, R. D. (1972). Paragenesis and isotopic composition of some gangue minerals from the uranium deposits of eldorado, saskatchewan. *Can. J. Earth Sci.* 9, 141–157. doi:10.1139/e72-012
- Sillitoe, R. H. (2010). Porphyry copper systems. *Econ. Geol.* 105, 3–41. doi:10.2113/gsecongeo.105.1.3
- Sun, J. (2015). *Magmaism and metallogenesis at Duolong ore district, Tibet*. Beijing: China University of Geosciences. doctoral thesis.
- Sun, J., Li, H., Liu, X., Xie, K., Chen, W., Xue, S., et al. (2015). Characteristics of chlorite from the tongkuangyu copper deposit in shanxi province and their geological implications. *Bull. Mineralogy, Petrology Geochem.* 34 (6), 1142–1154. (in Chinese with English abstract). doi:10.3969/j.issn.1007-2802.2015.06.007
- Sun, M., Tang, J., Klemd, R., Lin, B., Tang, P., Zhang, Z., et al. (2023). The formation of a giant post-collision porphyry copper system: a case study of the Jiamu deposit, Tibet. *GSA Bull.* doi:10.1130/B36924.1
- Tang, J., Ding, S., Meng, Z., Hu, G., Gao, Y., Xie, F., et al. (2016). The first discovery of the low sulfidation epithermal deposit in Linzizong volcanics, Tibet: a case study of the Sinongduo Ag polymetallic deposit. *Acta Geosci. Sin.* 37, 461–470. doi:10.3975/cagsb.2016.004.08
- Tang, J., Sun, X., Ding, S., Wang, Q., Wang, Y., Yang, C., et al. (2014). Discovery of the epithermal deposit of Cu (Au-Ag) in the Duolong ore concentrating area, Tibet. *Acta Geosci. Sin.* 35 (1), 6–10. (in Chinese with English abstract). doi:10.3975/cagsb.2014.01.02
- Tang, J., Wang, Q., Yang, H., Gao, X., Zhang, Z., and Zou, B. (2017). Mineralization, exploration and resource potential of porphyry-skarn-epithermal copper polymetallic deposits in Tibet. *Acta Geosci. Sin.* 38 (5), 571–613. doi:10.3975/cagsb.2017.05.02
- Tang, N. (2022). The construction of an alteration mineral exploration model for porphyry mineralization systems based on short-wave infrared spectroscopy: a case study of Qulong porphyry deposit in Tibet. Chengdu: Chengdu University of Technology. doctoral thesis.
- Tindle, A. (2010). *Chlorite formula unit calculator and variety namer*. Available at: http://www.open.ac.uk/earth-research/tindle/AGT/AGT_Home_2010/Microprobe-2.html
- Vidal, O., Lanari, P., Munoz, M., Bourdelle, F., and De Andrade, V. (2016). Deciphering temperature, pressure and oxygen-activity conditions of chlorite formation. *Clay Min.* 51, 615–633. doi:10.1180/claymin.2016.051.4.06
- Vidal, O., and Parra, T. (2000). Exhumation paths of high-pressure metapelites obtained from local equilibria for chlorite-phengite assemblages. *Geol. J.* 35, 139–161. doi:10.1002/gj.856
- Vidal, O., Parra, T., and Trotet, F. (2001). A thermodynamic model for FE-MG aluminous chlorite using data from phase equilibrium experiments and natural pelitic assemblages in the the 100° to 600°C, 1 to 25 kb range. *Am. J. Sci.* 301, 557–592. doi:10.2475/ajs.301.6.557
- Walshe, J. L. (1986). A six-component chlorite solid solution model and the conditions of chlorite formation in hydrothermal and geothermal systems. *Econ. Geol.* 81, 681–703. doi:10.2113/gsecongeo.81.3.681
- Wang, Q., Tang, J., Chen, Y., Hou, J., and Li, Y. (2019). The metallogenetic model and prospecting direction for the Duolong super large copper (gold) district, Tibet. *Acta Petrol. Sin.* 35 (03), 879–896. (in Chinese with English abstract). doi:10.18654/1000-0569/2019.03.16
- Wang, X., Mao, J., Cheng, Y., Zhang, X., Liu, P., Liu, S., et al. (2014). Characteristics of chlorite from the Xinliadong Cu polymetallic deposit in eastern Guangdong Province and their geological significance. *Acta Petrologica Mineralogica* 33 (5), 885–905. (in Chinese with English abstract).
- Wang, Z. Q., Chen, B., Yan, X., and Li, S. W. (2018). Characteristics of hydrothermal chlorite from the Niujuan Ag-Au-Pb-Zn deposit in the north margin of NCC and implications for exploration tools for ore deposits. *Ore Geol. Rev.* 101, 398–412. doi:10.1016/j.oregeorev.2018.08.003
- Wang, Y., Lin, J., Hu, Z., Wang, F., Pang, Y., and Gao, F. (2018). Characteristics of chlorite in Yunji deposit of Xiangshan uranium ore-field and its geological implication. *Uranium Geol.* 34 (3), 153–158. (in Chinese with English abstract). doi:10.3969/j.issn.1000-0658.2018.03.004
- Wiewióra, A., and Weiss, Z. (1990). Crystalliochemical classifications of phyllosilicates based on the unified system of projection of chemical composition: II. The chlorite group. *Clay Min.* 25, 83–92. doi:10.1180/claymin.1990.025.1.09
- Wilkinson, J. J., Chang, Z., Cooke, D. R., Baker, M. J., Wilkinson, C. C., Inglis, S., et al. (2015). The chlorite proximit: a new tool for detecting porphyry ore deposits. *J. Geochem. Explor.* 152, 10–26. doi:10.1016/j.gexplo.2015.01.005
- Wu, D., Pan, J., Xia, F., Huang, G., Zhong, F., Qi, J., et al. (2018). Characteristics and formation conditions of chlorite in the Shangjiao uranium deposit in the Southern Jiangxi Province, China. *Acta Mineral. Sin.* 38 (4), 393–405. (in Chinese with English abstract). doi:10.16461/j.cnki.1000-4734.2018.38.206
- Xiao, B., and Chen, H. (2020). Elemental behavior during chlorite alteration; new insights from a combined EMPA and LA-ICPMS study in porphyry Cu systems. *Chem. Geol.* 543, 119604. doi:10.1016/j.chemgeo

- Xiao, B., Chen, H., Hollings, P., Zhang, Y., Feng, Y., and Chen, X. (2020). Chlorite alteration in porphyry Cu systems: new insights from mineralogy and mineral chemistry. *Appl. Clay Sci.* 190, 105585. doi:10.1016/j.clay.2020.105585
- Xiao, B., Chen, H. Y., Hollings, P., Wang, Y. F., Yang, J. T., and Wang, F. Y. (2018a). Element transport and enrichment during propylitic alteration in Paleozoic porphyry Cu mineralization systems: insights from chlorite chemistry. *Ore Geol. Rev.* 102, 437–448. doi:10.1016/j.oregeorev.2018.09.020
- Xiao, B., Chen, H. Y., Wang, Y. F., Han, J. S., Xu, C., and Yang, J. T. (2018b). Chlorite and epidote chemistry of the Yandong Cu deposit, NW China: metallogenetic and exploration implications for Paleozoic porphyry Cu systems in the Eastern Tianshan. *Ore Geol. Rev.* 100, 168–182. doi:10.1016/j.oregeorev.2017.03.004
- Xiao, Z., Ouyang, Z., Lu, H., and Cheng, J. (1993). The characteristics of chlorites in the wall-rock alteration zone in the Baoban gold field, Hainan Island with the physico-chemical conditions of hydrothermal alteration. *Acta Mineral. Sin.* 13 (04), 319–324. (in Chinese with English abstract). doi:10.16461/j.cnki.1000-4734.1993.04.005
- Xie, X., Byerly, G. R., and Ferrell, R. E. (1997). Ilb trioctahedral chlorite from the Barberton greenstone belt; crystal structure and rock composition constraints with implications to geothermometry. *Contrib. Mineral. Petr.* 126, 275E–291E. doi:10.1007/s004100050250
- Xu, X., Zhang, S., Yang, C., Qin, Y., Ruan, X., and Peng, R. (2017). Characteristics of chlorite and its forming environment in the granitoid porphyry of southern of Xiangshan. *Jiangxi Sci.* 35 (2), 183–190. (in Chinese with English abstract). doi:10.13990/j.issn1001-3679.2017.02.001
- Yang, C., Tang, J., Song, J., Zhang, Z., Li, Y., Sun, X., et al. (2015). Chlorite characteristic of the Naruo porphyry Cu (Au) deposit in Tibet and its geological significance. *Acta Geol. Sin.* 89 (5), 856–872. (in Chinese with English abstract).
- Yang, Z., Hou, Z., Song, Y., Li, Z., Xia, D., and Pan, F. (2008). Qulong superlarge porphyry Cu deposit in Tibet: geology alteration and mineralization. *Mineral. Deposits* 27 (03), 279–318. (in Chinese with English abstract). doi:10.16111/j.0258-7106.2008.03.01
- Yang, Z., Xie, Y., Li, G., and X, J. (2005). Characteristics and forming process of ore-forming fluids at Qulong copper deposit in Gangdise porphyry copper belt, Tibet. *Geol. Prospect.* 42 (02), 21–26. (in Chinese with English abstract).
- Yavuz, F., Kumral, M., Karakaya, N., Karakaya, M. Ç., and Yıldırım, D. K. (2015). A Windows program for chlorite calculation and classification. *Comput. Geosci-Uk* 81, 101–113. doi:10.1016/j.cageo.2015.04.011
- Yin, A., and Harrison, T. M. (2000). Geologic evolution of the himalayan-Tibetan orogen. *Annu. Rev. Earth Pl. Sc.* 28, 211–280. doi:10.1146/annurev.earth.28.1.211
- Zane, A., and Weiss, Z. (1998). A procedure for classifying rock-forming chlorites based on microprobe data. *Rendiconti Lincei* 9, 51–56. doi:10.1007/BF02904455
- Zhang, J., Chen, P., Wang, K., Liu, X., Chen, Q., Huang, J., et al. (2018). The relationship between chlorite and uranium mineralization of granites in south China. *J. East China Univ. Technol.* 41 (2), 134–138. (in Chinese with English abstract). doi:10.19540/j.cnki.cjcm.20171027.005
- Zhang, S., He, W., Gao, X., Zhang, H., Yuan, J., and Jianjiang, Y. (2020a). Ore-forming fluids evolution of the porphyry Cu deposits: alteration mineralogy and thermodynamic modeling of the Pulang Cu deposit, Zhongdian district. *Acta Petrol. Sin.* 36 (05), 1611–1626. (in Chinese with English abstract). doi:10.18654/1000-0569/2020.05.18
- Zhang, S., Xiao, B., Long, X., Chu, G., Cheng, J., Zhang, Y., et al. (2020b). Chlorite as an exploration indicator for concealed skarn mineralization: perspective from the Tonglushan Cu–Au–Fe skarn deposit, Eastern China. *Ore Geol. Rev.* 126, 103778. doi:10.1016/j.oregeorev.2020.103778
- Zhang, W., Zhang, S., Cao, H., Wu, J., Xiao, C., Chen, H., et al. (2014). Characteristics of chlorite minerals from Xiaolonghe tin deposit in West Yunnan, China and their geological implications. *J. Chengdu Univ. Technol. Sci. Technol. Edi-tion* 41 (03), 318–328. (in Chinese with English abstract). doi:10.3969/j.issn.1671-9727.2014.03.08
- Zhang, Z., Hua, R., Ji, J., Zhang, Y., Guo, G., and Yin, Z. (2007). Characteristics and formation conditions of chlorite in No. 201 and No. 361 uranium deposits. *Acta Mineral. Sin.* 27 (2), 161–172. (in Chinese with English abstract). doi:10.16461/j.cnki.1000-4734.2007.02.011
- Zheng, Z., Chen, F., and Yu, X. (1997). Characteristics of chlorite in Baguamiao gold deposit and their geological significance. *Acta Mineral. Sinica* 17 (01), 100–106. (in Chinese with English abstract). doi:10.16461/j.cnki.1000-4734.1997.01.016
- Zhong, R., Li, W., Chen, Y., and Huo, H. (2012). Ore-forming conditions and genesis of the Huogeqi Cu–Pb–Zn–Fe deposit in the northern margin of the North China Craton: evidence from ore petrologic characteristics. *Ore Geol. Rev.* 44, 107–120. doi:10.1016/j.oregeorev.2011.09.008
- Zhou, D., Zhao, T., Zhao, P., and Zhang, X. (2018). Chlorite EPMA characteristic and its geological significance of the Kangshan Au–Ag–Pb–Zn deposit in west of Henan. *Mineral. Explor.* 9 (5), 803–824. (in Chinese with English abstract).
- Zhu, X., Chen, H., Liu, H., Ma, D., Li, G., Huang, H., et al. (2015). Zircon U–Pb ages, geochemistry of the porphyries from the duobuza porphyry Cu–Au deposit, Tibet and their metallogenetic significance. *Acta Geol. Sin.* 89 (03), 534–548. (in Chinese with English abstract). doi:10.19762/j.cnki.dizhixuebao.2015.01.009
- Zhu, X. P., Ji, D., Li, G. M., Liu, H. F., Liu, C., Chen, H., et al. (2019). High oxidation magmatic evolution in the Naruo porphyry Cu deposit, Tibet, China. *Gondwana Res.* 76, 26–43. doi:10.1016/j.gr.2019.05.006